

AD-A136 964

TIME-DEPENDENT CHILD-LANGMUIR DIODE SIMULATION(U)  
CALIFORNIA UNIV BERKELEY ELECTRONICS RESEARCH LAB  
S ROUSSET 11 JUL 83 UCB/ERL-M83/39 N00014-77-C-0578

1/1

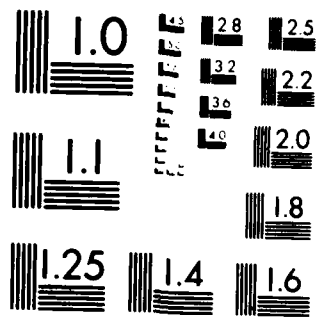
UNCLASSIFIED

F/G 12/1

NL



END
DATE
FORMED
2 84
DTIC



MICROCOPY RESOLUTION TEST CHART  
NATIONAL BUREAU OF STANDARDS 1963-A

AD A136964

Contract N00014-77-C-0578

TIME-DEPENDENT CHILD-LANGMUIR DIODE SIMULATION

by  
Stephane Rousset

Memorandum No. UCB/ERL M83/39

11 July 1983

ELECTRONICS RESEARCH LABORATORY  
College of Engineering  
University of California, Berkeley  
94720

This document has been approved  
for public release and sale; its  
distribution is unlimited.

# Time-Dependent Child-Langmuir Diode Simulation

*Stéphane Rousset*

## ABSTRACT

*The*

A one-dimensional numerical code has been written, which allows the time-dependent simulation of the Child-Langmuir diode and the plasma sheath problem. Our model assumes a semi-infinite plasma reservoir from which particles can be emitted into a vacuum region where they can be accelerated or decelerated by means of an external potential on the anode, until they are eventually absorbed by the anode or sent back to the reservoir.

Physical results are shown for both the time-independent and the time-dependent cases. Numerical methods are presented for the evaluation of relevant physical quantities. The numerical effects are discussed.

Accession For		
NTIS GRA&I	<input checked="" type="checkbox"/>	
DTIC TAB	<input type="checkbox"/>	
Unannounced	<input type="checkbox"/>	
Justification	<i>per</i>	
By _____		
Distribution/		
Availability Codes		
Dist	Avail and/or	
	Special	
<i>A-1</i>		



### ACKNOWLEDGMENTS

We would like to acknowledge Professor Charles K. Birdsall and Dr. Thomas L. Crystal in the Electronics Research Laboratory at the University of California at Berkeley for their advice, help, suggestions and overall assistance in all stages of design, writing and testing of our code. Credit should also be given to Dr. A. Bruce Langdon at the Lawrence Livermore National Laboratory for being the author of the ES1 code from which our own program is derived. Also, we would like to thank William Lawson for his help in obtaining theoretical solutions to the steady-state diode. Bettina Wiskott also deserves many thanks for her help in drawing most of the figures.

This project and the following report were partially supported by the Office of Naval Research under Contract No. N00014-77-C-0578, and in part by the Department of Energy under Contract No. DE-AT03-76ET53064.

The computational portion of this work was supported by the National Magnetic Fusion Energy Computer Center at Lawrence Livermore National Laboratory. This report has been written using the UNIX† time-sharing system operated by the Computing Services at the University of California at Berkeley.

Editorial Note (C. K. Birdsall): This is the initial report on simulation of *bounded* plasmas from our Plasma Theory and Simulation Group. It represents an appreciable step for us, *away* from the usual initial-value, spatially periodic, overall-neutral particle models, and *into* boundary-value, non-neutral plasma models with particle emission and collection, and with external circuits, applied currents and voltages. Hence, S. Rousset had to invent and implement a variety of injection, diagnostic, and graphical presentation techniques. The results are excellent as the reader may see. We are still trying to understand fully the physics recovered herein and this report should be considered as describing *work in progress*. The work was begun before I went on sabbatical leave and, while I was away, ably supported by Dr. T. L. Crystal through to completion.

---

† UNIX is a Trademark of Bell Laboratories.

CONTENTS

1.	INTRODUCTION	4
2.	MODELS	5
2.1.	Physical Model	5
2.2.	Numerical Model	5
2.2.1.	The Main Frame	5
2.2.2.	Non-Neutral Conditions	6
3.	THE PLOUF CODE	7
3.1.	General Structure	7
3.2.	Initialization	7
3.2.1.	SETVNU	7
3.2.2.	SETXNU	9
3.3.	FIELDS	9
3.4.	ACCEL	10
3.5.	MOVE	10
3.5.1.	Computation of the Charge Fluxes	10
3.5.1.1.	The $j=\rho v$ Method	11
3.5.1.2.	The $i=dq/dt$ Method	11
3.5.1.3.	Current Measurements.	11
3.5.2.	Computation of the Displacement Currents	12
3.6.	REPACK	12
3.7.	ENTER	12
3.8.	Input Parameters	13
3.9.	Diagnostics	13
3.9.1.	Snapshots	13
3.9.2.	History Plots	14
4.	RESULTS	15
4.1.	Numerical Results	15
4.1.1.	Initial Velocity Distribution and Noise	15
4.1.2.	Oscillations of $\Phi_{\min}$ (driftless case)	15
4.1.3.	Time-Dependence of the Current	16
4.1.3.1.	Current Noise	16
4.1.3.2.	Current Oscillations	16
4.2.4.	Cost of the Pad-Cells	16
4.2.	Physical Results	17
4.2.1.	Vacuum Diode	17
4.2.2.	Reaching Equilibrium	17
4.2.3.	Temperature Effects	18
4.2.4.	Effect of $\Phi_0$ on the Velocity Distribution	19
4.2.5.	$i=i(\Phi_0)$ Characteristic	19
5.	CONCLUSION	20

## 1. INTRODUCTION

The growing interest in many different disciplines for diode-like problems, along with the highly nonlinear behavior of such configurations, have stimulated the search for solutions to these problems by means of numerical simulation.

Scientists in the fields of plasma physics and space sciences are especially interested in the results of such simulations, since our problem has direct applications in the domains of Q-machines, plasma-surface interactions and effects of the first wall on the plasma within a fusion reactor, plasma insulators, Langmuir probes, probe-wall effects, etc.

The general purpose of the study is to simulate the behavior of the plasma sheath by means of a unidimensional numerical code, in order to reach by simulation the essence of the physics of this problem. Our goal in this project was to build and test the tool (a numerical code) necessary for such a search.

Many people have studied diode-like problems analytically, experimentally and computationally: see Child (1911), Langmuir (1923), Pierce (1948), Tien & Moshman (1956), Self (1963), Birdsall & Eridges (1966), Kuhn (1979). In their classic paper, I. Langmuir and H. Mott-Smith (1924) studied the time-independent solution of the diode problem. However, the stability of this solution was not described and several questions had not been answered: was there some kind of oscillating mode, or was the equilibrium perfectly time-independent? And in case such an oscillation existed, was the time-independent solution just the time-average of the oscillation?

In our study, we have been especially interested in measuring the numerical effects due to the model we chose; the idea was that a good knowledge of such effects is necessary for a correct interpretation of the results, in order to distinguish between the real physical results and the artificial numerical effects. Once we were able to make this distinction, we used our code to simulate some well-known configurations, so as to get more insight into the physics of a plasma sheath.

In this report, we first present our physical and numerical models; we then devote a substantial part to the numerical methods used; we conclude with the study of numerical and physical effects.

## 2. MODELS

### 2.1. Physical Model

Figure 1 shows the configuration we will study here; it can be described as follows: the half-space  $x < 0$  (we treat the unidimensional case) consists of a plasma reservoir filled with particles of one or several species; we assume that the velocity distributions of each species in the reservoir are Maxwellian (with a possible drift) in the neighborhood of  $x=0$ . A target is placed at  $x=L > 0$ , which absorbs perfectly any incident particle (no secondary emission). Between  $x=0$  and  $x=L$ , we have a vacuum background, plus (possibly) particles emitted from the plasma reservoir.

The virtual wall at  $x=0$  is assumed to be at zero potential; an external potential difference  $\Phi_0$  can be applied between  $x=0$  and  $x=L$ .  $\Phi_0$  can take any value and can be time-dependent. Furthermore, there can be a net current.

We do not add possible collisions between particles. No gravitational field is present. Unless otherwise specified, particles are electrons. No magnetic field is present.

As a consequence of the above configuration and assumptions, we can expect the following general behavior: particles are moving about due to their own and applied fields; depending on the charge density within the vacuum region, depending on the externally applied potential, and depending on its initial velocity, a particle contributes to the cathode ( $x=0$ ) or anode ( $x=L$ ) charge flux, or it remains between the boundaries. It is the collective behavior of such particles, the resulting fields, currents, energies, etc. that the PLOUF code allows us to study.

### 2.2. Numerical Model

This paragraph should give the reader a global idea of the general structure of the PLOUF code, without entering too many details at this time. We should point out here that our code owes its structure and much of its actual programming to the ES1 code written by A. B. Langdon. In this report, we will assume that the reader has some previous knowledge of this code or has access to the relevant literature.

#### 2.2.1. The Main Frame

Since we are studying time-varying phenomena using a digital computer (as opposed to an analog computer), some kind of discretization of time has to be introduced: the basic assumption is that, by knowing what happens at a finite number of instants, we will know the continuous evolution of the variables. Our code (as well as ES1) proceeds as follows: knowing the positions and charges of the particles at some time  $t$  (and the velocities at  $t-\Delta t/2$ ), we can evaluate the fields at that time  $t$ , deduce the accelerations, find the new velocities at time  $t+\Delta t/2$ , calculate the new positions at  $t+\Delta t$ , and so on.

Consequently, the main frame of the code can be very roughly described like this:

- 1 Initialize (includes:  $t=0$ ;  $timestep=\Delta t$ ; duration of simulation  $t_{end}$ ; definition of spatial grid; put particles in their places in phase-space).
- 2 Compute fields (from charge density  $\rho$ ).
- 3 Compute velocities of particles.
- 4 Compute positions of particles.
- 5  $t=t+\Delta t$ .
- 6 If  $t < t_{end}$ , then go to line 2.
- 7 End.

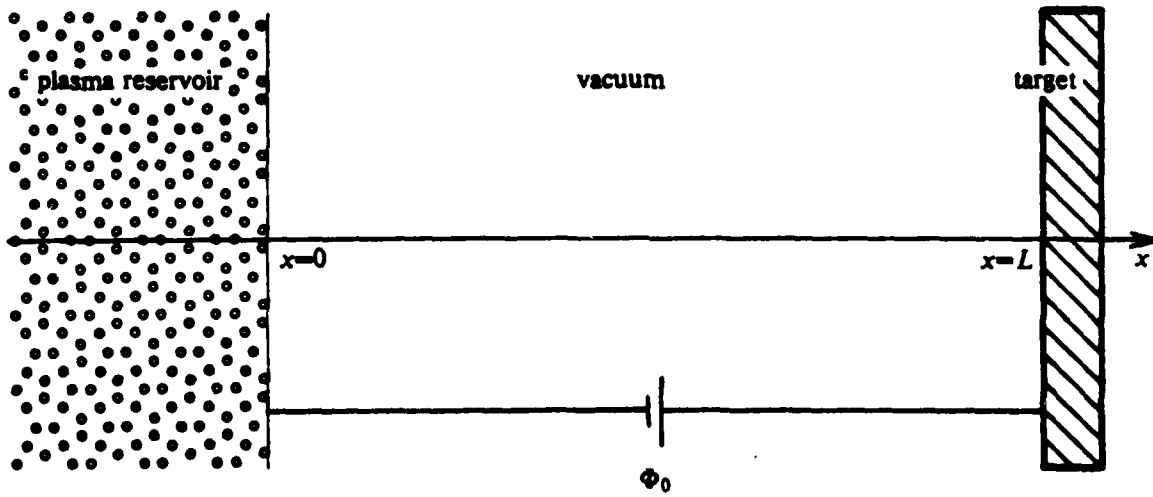


Figure 1 (Section 2.1): Physical model.

### 2.2.2. Non-Neutral Conditions

The ES1 code is designed for the simulation of periodic, infinite configurations, with no net charge or field:  $\langle \rho \rangle = 0$  and  $\langle E \rangle = 0$ . It does not include any source or sink of particles. However, we see from the physical model described in Section 2.1 that in our problem particles can enter or leave the sheath (i.e., they appear to be created or destroyed). In order to allow for a non-neutral plasma, we let the simulation region extend from  $x=0$  to  $x=2L$ , and consider that our true sheath is from  $x=0$  to  $x=L$ , and assume that the remaining half is a fake sheath. In the first region, we compute the charge density  $\rho$  from the particle positions. Then, we add an inverted charge density in the fake region, so that  $\rho(L+x) = -\rho(L-x)$ . This modification means that we have  $\rho(0) = \rho(2L)$ , so that the periodicity requirement  $E(x+2L) = E(x)$  for the Fourier transforms in ES1 is satisfied. Note that this modification is equivalent to considering that, for each charge at  $x=x_0$  in the true sheath, there is an image charge of opposite sign at  $x=2L-x_0$  in the fake region.

Once we know the charge density  $\rho(x)$  in the whole sheath, we can evaluate the fields for  $0 < x \leq 2L$ , using Poisson's equation; then we add the externally applied potential  $\Phi_0$  between  $x=0$  and  $x=L$ , as a solution to the homogeneous (Laplace) equation.

The existence of a plasma reservoir for  $x < 0$  is accounted for by the creation of particles with positive velocities at  $x=0$ , and by the absorption of particles with negative velocities at  $x=0$  and with positive velocities at  $x=L$ . (In fact, this absorption does not occur exactly at  $x=0$  and  $x=L$ ; see Section 3.2.2.)

Note that there are no particles in the fake sheath, so that the existence of this region increases the computation costs only in the doubling of the region over which the fields are solved (in other words, there is no doubling of the number of particles).

With the above features, PLOUF is basically ready to run.

### 3. THE PLOUF CODE

#### 3.1. General Structure

PLOUF performs some tasks added to ES1, such as: inject new particles in the diode, compute currents, deal with the variable number of particles in the system.

Consequently, the main frame of our code looks like this:

- 1 Initialize (includes:  $t=0$ ;  $timestep=\Delta t$ ; duration of simulation  $t_{end}$ ; definition of spatial grid; load particles in phase-space at  $t=0$ ; load entering particles in their own phase-space).
- 2 Compute fields (from charge density  $\rho$ ), and evaluate the displacement currents near the boundaries.
- 3 Compute velocities of particles.
- 4 Compute positions of particles.
- 5 Compute currents everywhere (at some selected time steps) and at the boundaries (at each time step).
- 6 Repack arrays representing particles (if applicable).
- 7 Load entering particles.
- 8  $t=t+\Delta t$ .
- 9 If  $t < t_{end}$ , then go to line 2.
- 10 End.

#### 3.2. Initialization

The INIT subroutine performs two tasks. First, it sets up the state of the system at the start of the simulation by loading particles in phase-space according to the relevant input parameters. This set of operations is performed exactly as in ES1; it should be noted that the initialization stage is not of primary concern to us, since our problem is essentially a boundary-value problem (not an initial-value problem like ES1).

The second task is to load the new, entering particles in phase-space. Specifying how many particles will enter the system during each time step, we set up (in SETVNU) a discrete distribution of velocities for these particles. Then, we compute (in SETXNU) the corresponding initial positions, which cannot be merely  $x=0$ , due to the method we use for computing the currents at the boundaries.

##### 3.2.1. SETVNU

According to our physical model (see section 2.1), particles in the reservoir  $x < 0$  have a (possibly drifting) Maxwellian distribution of velocities. Under this assumption, the purpose of SETVNU is to compute, for each species independently, the velocities of the particles entering the system at each time step, given the following parameters:

*nenter* the number of particles  $n_{new}$  in the distribution;  
*vinth* the thermal velocity  $v_{th}$  of the distribution;  
*vinbim* the drift velocity  $v_b$  of the distribution;  
*vinmin* the smallest velocity  $v_{min}$  in the distribution;  
*vinmax* the largest velocity  $v_{max}$  in the distribution. (These last two parameters allow retaining only a "slice" of the whole Maxwellian.)

Let us see how these *nenter* velocities are computed. In the cold case, i.e.  $v_{th}=0$ , the result is trivial:

$$v_{new}(i) = v_b, \quad i=1, n_{new}.$$

In the warm case, the task is more complex. Lets consider that we have the following normalized Maxwellian distribution in the reservoir  $x < 0$ :

$$f(v_{new}) dv_{new} = \frac{1}{\sqrt{\pi} v_{th}} e^{-\frac{(v_{new}-v_b)^2}{v_{th}^2}} dv_{new}$$

Then the distribution function for emission (i.e. the probability to observe during  $\Delta t$  a particle passing through  $x=0$  with a velocity between  $v_{new}$  and  $v_{new}+dv_{new}$ , with  $v > 0$ ) is:

$$g(v_{new}) dv_{new} = \frac{A n_{new}}{\sqrt{\pi} v_{th}} v_{new} e^{-\frac{(v_{new}-v_b)^2}{v_{th}^2}} dv_{new} \quad (1)$$

where  $A$  is a normalization constant defined by:

$$\int_{v_{min}}^{v_{max}} g(v_{new}) dv_{new} = n_{new}$$

Changing variables,  $x = v_{new} - v_b$ , we obtain:

$$A = 2 \left\{ \frac{v_{th}}{\sqrt{\pi}} \left[ e^{-\frac{(v_{min}-v_b)^2}{v_{th}^2}} - e^{-\frac{(v_{max}-v_b)^2}{v_{th}^2}} \right] + v_b \left[ \operatorname{erf} \left( \frac{v_{max}-v_b}{v_{th}} \right) - \operatorname{erf} \left( \frac{v_{min}-v_b}{v_{th}} \right) \right] \right\}^{-1}$$

Now that  $g(v)dv$  is specified, SETVNU executes the following algorithm, which constructs a set of *newer* velocities satisfying Equation 1:

- 1 Initialize:  $i=1$
- 2 Compute the integral of the distribution function  $g(v)dv$  from zero to the velocity of the slowest particle to be injected; this will give the value of the integral corresponding to the smallest velocity in the distribution function for entering particles:

$$I_{min} = \int_0^{v_{min}} g(v_{new}) dv_{new} = \frac{1}{n_{new} + 1}$$

- 3 Compute the value of the integral of  $g(v)dv$  which corresponds to the next higher velocity in the distribution:

$$I = I_{min} + \frac{2i}{n_{new} + 1}$$

- 4 Using Newton's method, compute the velocity corresponding to the value of the integral that we just found in Step 3; that is, find  $v$  such that  $\int_0^v g(v_{new}) dv_{new} = I$
- 5 Prepare next step:  $i=i+1$
- 6 If  $i \leq n_{new}$ , then go to line 3
- 7 End

In Step 4 above, using Newton's method implies having some knowledge of an initial approximation  $v_0(i)$  to the solution  $v_{new}(i)$ . The safest way to go, when  $i=1$ , is to start with

$$v_0(i) = \frac{v_b + \sqrt{v_b^2 + 2v_{th}^2}}{2},$$

i.e. the velocity for which  $g(v_{new})$  is maximum. This way, Newton's method converges even for sharply peaked distributions (without becoming too costly in terms of computing time). Subsequently, for  $i > 1$ , we just take  $v_0(i) = v_{new}(i-1)$ .

### 3.2.2. SETXNU

The SETXNU subroutine computes the positions of the entering particles; these positions are computed according to the following three criteria:

- \* all new particles must pass  $x=0$  regularly in time; this means for instance that the  $i$ th particle of one group must enter the diode at time  $t+\Delta t\{(i-1)/nenter\}$  (assuming that we have one single species). Note: we call "group" a set of  $nenter$  particles of one or several species, due to enter the diode during one time step of the simulation.
- \* all species must be treated simultaneously within one group; e.g.: if we have two species with  $nenter_1=2nenter_2$ , then we will first load two particles of species 1, then one particle of species 2, then two particles of species 1, . . . , until  $nenter_1+nenter_2$  particles have been loaded for the given time step.
- \* no particle may be loaded at  $x > -\Delta x/2$ ; this is due to our method of current measurements.

On the left-hand side of Figure 2, we show the positions of the particles when they are loaded in phase-space, assuming (for the sake of simplicity) that the distribution function for emission is such that the free-streaming particles form a straight line in phase-space. Under this assumption, the distribution function tells us that the particles are to be loaded along a straight line in phase-space. However, it does not tell us either the slope or the position of this line, which are determined as follows:

- \* the position of the line (its offset in the  $x$ -direction once the slope is known) must be such that the slowest particle is loaded at a position  $x(t_0) \approx -\Delta x/2$ , where  $t_0$  is the loading time;
- \* calling  $n$  the number of time steps needed for the slowest particle to enter the sheath from its loading position, then the slope of the straight line must ensure that exactly one particle passes  $x=0$  at time  $t_0+n\Delta t+\Delta t/nenter$ , exactly one particle passes  $x=0$  at time  $t_0+n\Delta t+2\Delta t/nenter$ , . . . , and exactly one particle passes  $x=0$  at time  $t_0+n\Delta t+nenter\Delta t/nenter$ .

The curve on the right-hand side of Figure 2 (the curve located inside the diode region) shows the positions of the particles in phase-space at time  $t_0+(n+1)\Delta t$ , i.e. at the end of the time step during which they enter the sheath.

Figure 3 is similar to Figure 2, except that it corresponds to a Maxwellian distribution function in the reservoir.

### 3.3. FIELDS

The subroutine FIELDS has been modified so as to construct the inverted charge density in the fake sheath, and to add the externally applied potential. For further explanations, please read Section 2.2.2.

This subroutine also computes the displacement currents near the boundaries, i.e.  $J_{disp}(\Delta x)$  and  $J_{disp}(L-\Delta x)$ :

$$J_{disp}(\Delta x) = \frac{E(\Delta x, t+\Delta t) - E(\Delta x, t)}{\Delta t}$$

$$J_{disp}(L-\Delta x) = \frac{E(L-\Delta x, t+\Delta t) - E(L-\Delta x, t)}{\Delta t}$$

Please read Section 3.5.2 to see why we compute  $J_{disp}(\Delta x)$  and  $J_{disp}(L-\Delta x)$  instead of  $J_{disp}(0)$  and  $J_{disp}(L)$ .

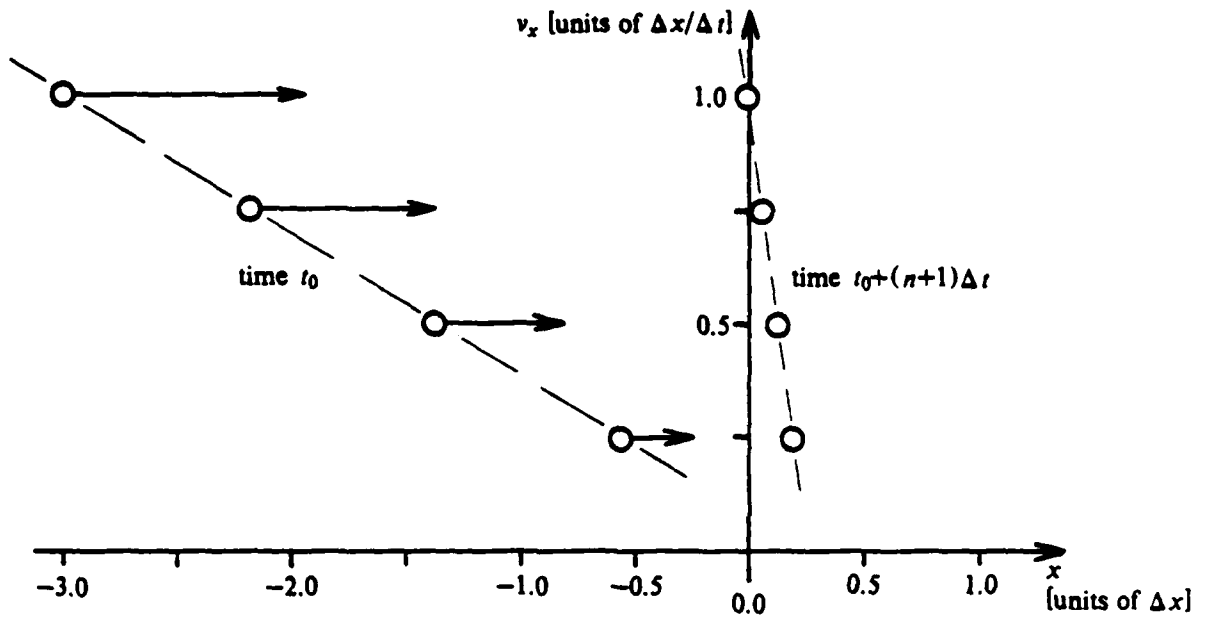


Figure 2 (Section 3.2.2): Loading of new particles (emission distribution function is a constant).

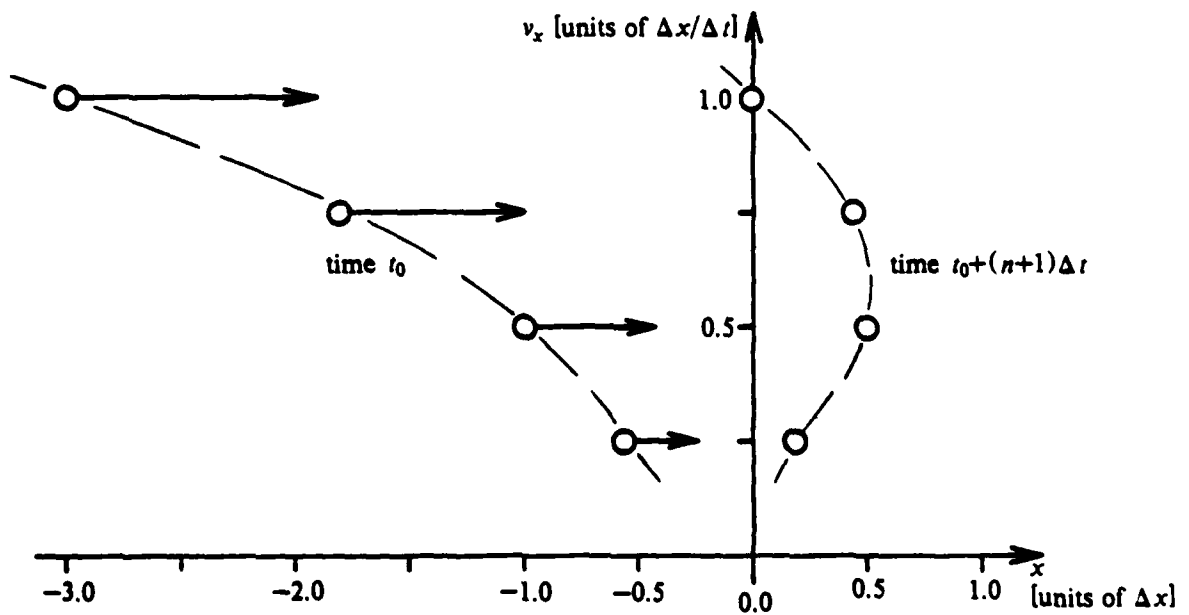


Figure 3 (Section 3.2.2): Loading of new particles (emission distribution function is Maxwellian).

### 3.4. ACCEL

The ACCEL subroutine computes the new velocities at time  $t+\Delta t/2$ .

Sections 3.5.1.2 and 3.5.1.3 explain how the currents are measured. A consequence of our method of loading new particles is that they are not exactly created and destroyed at  $x=0$  and  $x=L$ . They are in fact created at some  $x \leq -\Delta x/2$  and destroyed at  $x = -\Delta x/2$  and  $x = L + \Delta x/2$ . Of course, this slight modification with respect to our numerical model must not have any consequence on the behavior of physical quantities between  $x=0$  and  $x=L$ . The ACCEL subroutine takes care of this by keeping constant the velocities of the particles which are at positions  $x_0$  such that  $-\Delta x/2 \leq x_0 < 0$  or  $L \leq x_0 < L + \Delta x/2$ .

In other words, particles free stream when they are not strictly within the diode (i.e. when their positions  $x$  are not such that  $0 < x \leq L$ ). Note that this is an approximation, since we have finite-size particles, which should be accelerated proportionally to that fraction of the particle which is strictly within the diode.

Furthermore, ACCEL computes the drift and kinetic energies so that the contribution of a particle is multiplied by a factor which gives the percentage of the finite-size particle residing inside the diode:

$$part(x) = \min \left[ \max \left[ \frac{L+\Delta x}{2} - \left| \frac{L}{2} - x \right|, 1 \right], 0 \right]$$

This accounts for the gradual entrance of a finite-size particle in the diode, and it decreases the noise (in the energy calculations) due to particles exiting and entering the diode.

### 3.5. MOVE

The basic way of computing the new positions of the particles at each time step is trivial:  $x(t+\Delta t) = x(t) + v_x(t+\Delta t/2)\Delta t$ . The mover computes the new positions of all particles according to this relation, as in ES1.

In our code, MOVE has also a second function, which is to measure the charge fluxes (also called *ballistic currents*).

#### 3.5.1. Computation of the Charge Fluxes

There are different means of obtaining the ballistic currents. One method would be to compute  $j = \rho v$  knowing  $v$  at time  $t+\Delta t/2$  and evaluating  $\rho$  at the same time, using  $\rho(t)$  and  $\rho(t+\Delta t)$ . This method requires that we define some interface (some interpolation scheme) between the velocity, which is a particle quantity, and the charge density, which is a grid quantity; furthermore, we will see in Section 3.5.1.1 that this current does not satisfy Kirchhoff's law within any volume bounded by any pair of grid planes.

The method implemented in PLOUF measures  $i = dq/dt$ , i.e. the charge which has gone through the grid plane(s) on which we want to measure the charge flux.

At this point, please allow us to briefly recall some basic notions about particle shaping.

In order to evaluate the particle (and charge) density on the discrete spatial grid from the continuous particle positions, we infer that the particles have some finite size. We call *particle shaping* (or *particle weighting*) the process in which we define (on the grid) a particle density  $n(x)$  for each particle. Typically, the extent of a particle (i.e. the length of the interval on which  $n(x) \neq 0$ ) is one or two grid spaces.

### 3.5.1.1. The $j=\rho v$ Method

Now, let us examine the relation between the particle shaping and the measurement of the ballistic current via the first method ( $j=\rho v$ ).

We need to evaluate  $\rho_{t+\Delta t/2}$  on the basis of  $\rho_t$  and  $\rho_{t+\Delta t}$ . We can take  $\rho_{t+\Delta t/2}$  to be the time-average of the shapes  $\rho_t$  and  $\rho_{t+\Delta t}$  (see Figures 4 and 5):

$$\rho_{t+\Delta t/2}(X_j, x_t, x_{t+\Delta t}) \equiv \rho \left( X_j, \frac{x_t + x_{t+\Delta t}}{2} \right)$$

We can also define  $\rho_{t+\Delta t/2}$  as the space-average of  $\rho_t$  and  $\rho_{t+\Delta t}$  (see Figures 6 and 7):

$$\rho_{t+\Delta t/2}(X_j, x_t, x_{t+\Delta t}) \equiv \frac{\rho(X_j, x_t) + \rho(X_j, x_{t+\Delta t})}{2}$$

The advantage in using either one of these definitions is that we will measure instantaneous charge fluxes with a high accuracy. In fact, the time-averaging for  $\bar{\rho}(x_{t+\Delta t/2})$  would be required to insure self-consistency if we were to re-use these ballistic currents at some other place in the simulation (e.g. to compute new fields); in PLOUF, the currents are needed only for diagnostics.

The bad point is that this method does not provide for charge conservation within every volume bounded by an arbitrary choice of two planes. Indeed, looking at what happens for a high-velocity particle (Figures 2a and 3a), we see that there may be grid planes with no charge flux, even though in reality some charge has gone through it in one time step,  $\Delta t$ . In other words, Kirchhoff's law is not satisfied with this model, and there is no guarantee (especially for  $\text{randvx}=0$ ) that this adverse effect will become statistically negligible. Furthermore, some of the dynamics would probably be lost in the interface between charge densities and particle velocities.

### 3.5.1.2. The $i=dq/dt$ Method

The second method settles the problem of charge conservation, at the expense of some loss of information about current dynamics. This method computes the total charge flow through each grid plane during one time step:

$$i_{\text{measured}} \equiv \frac{\Delta q}{\Delta t} = \frac{1}{\Delta t} \int_t^{t+\Delta t} i_{\text{real}} dt.$$

where  $i_{\text{measured}}$  is defined on grid planes only:

$$i_{\text{measured}} \equiv i_{\text{measured}}(j\Delta x)$$

and  $i_{\text{real}}$  is the instantaneous charge flux at any given instant between  $t$  and  $t+\Delta t$ .

In order to achieve this evaluation of the current, we must use a current shape as defined by Figures 8 and 9. Using this shape and taking its values on the grid points, we have directly the values of the currents at these points.

### 3.5.1.3. Current Measurements

After having moved a particle, MOVE computes the ballistic currents associated with this particle; it then gives two results:

- \* values  $i(X_j, t)$  on all grid planes, at some selected time steps;
- \* boundary charge fluxes:  $i_{\text{emitter}}(t)$ ,  $i_{\text{cathode}}(t)$ ,  $i_{\text{anode}}(t)$ .

Like the accumulation of charge density, the computation of the current shapes is basically non-vectorizable, thus making MOVE quite expensive to use. However, we do not really

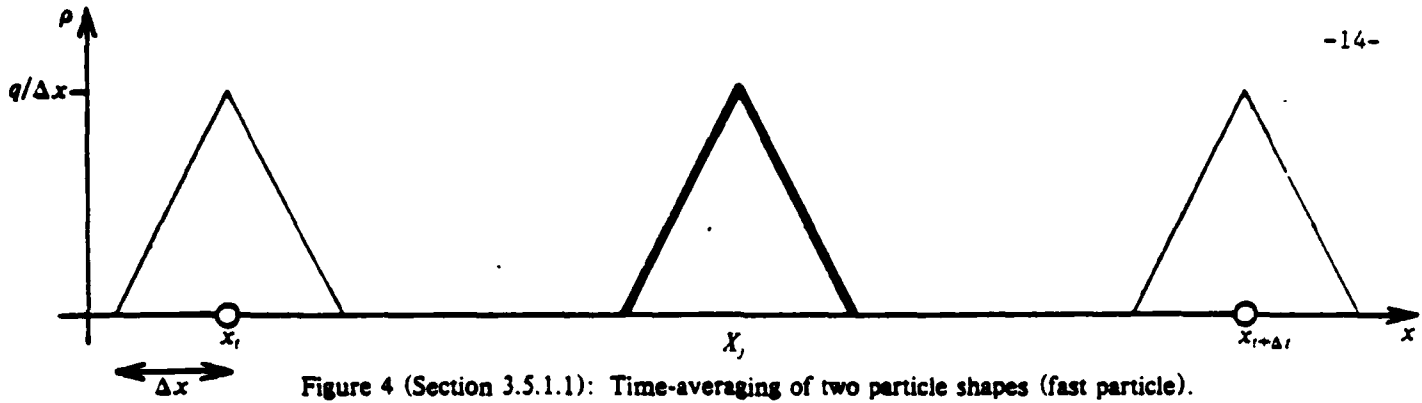


Figure 4 (Section 3.5.1.1): Time-averaging of two particle shapes (fast particle).

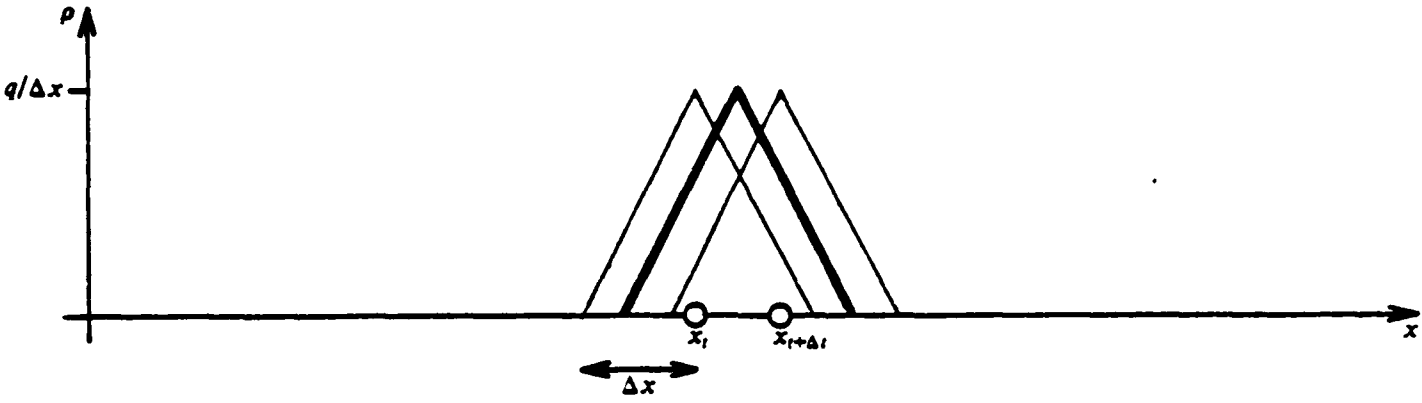


Figure 5 (Section 3.5.1.1): Time-averaging of two particle shapes (slow particle).

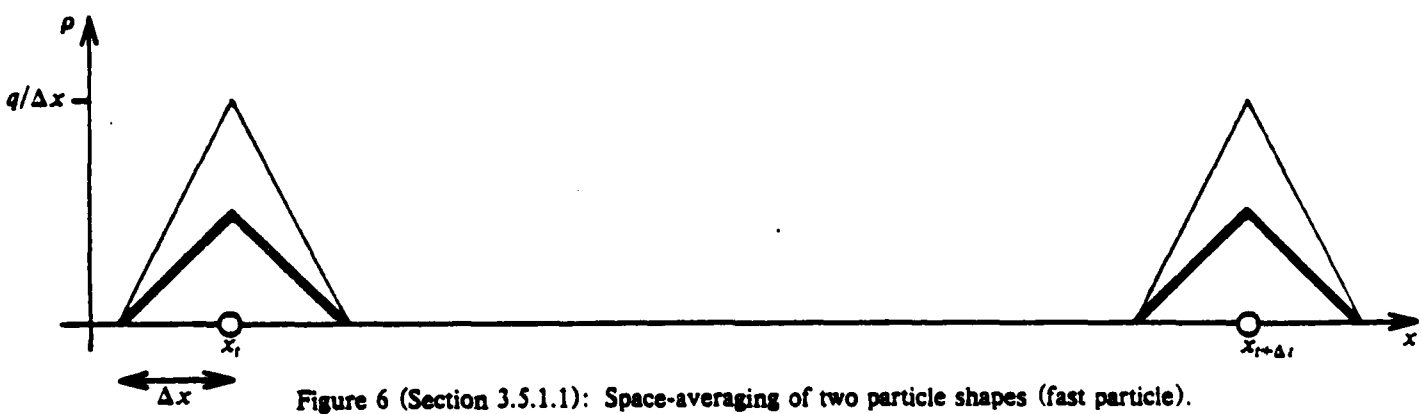


Figure 6 (Section 3.5.1.1): Space-averaging of two particle shapes (fast particle).

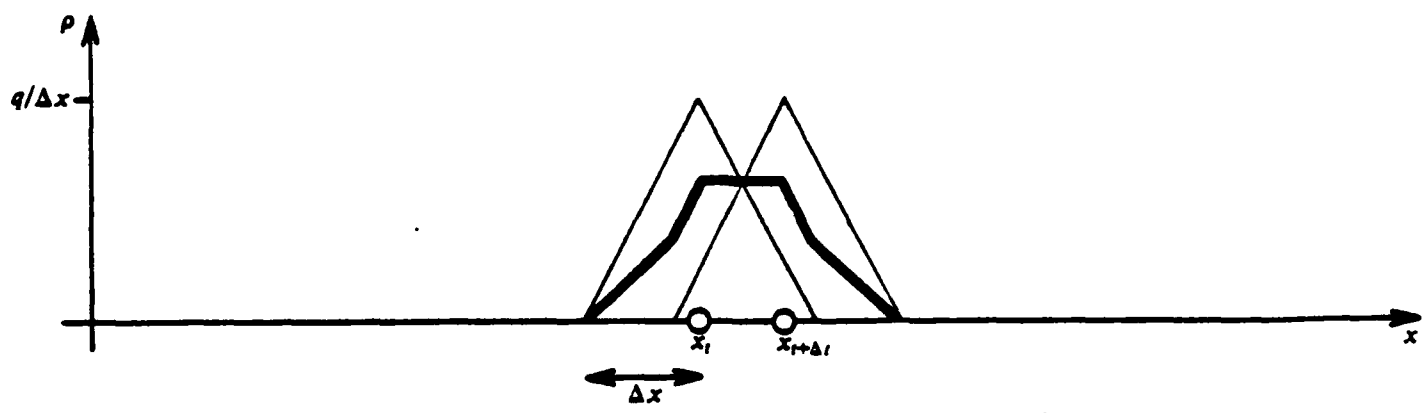


Figure 7 (Section 3.5.1.1): Space-averaging of two particle shapes (slow particle).

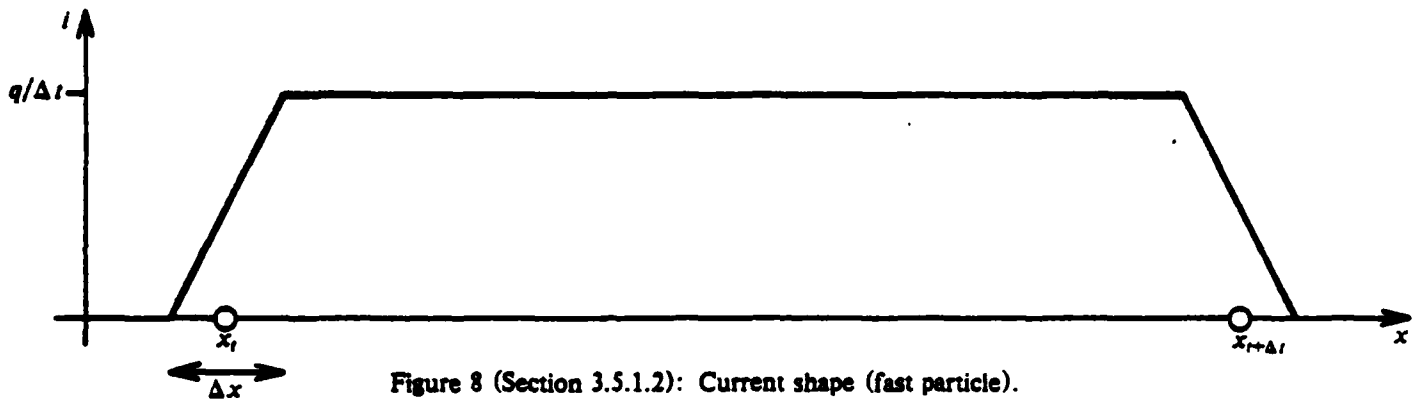


Figure 8 (Section 3.5.1.2): Current shape (fast particle).

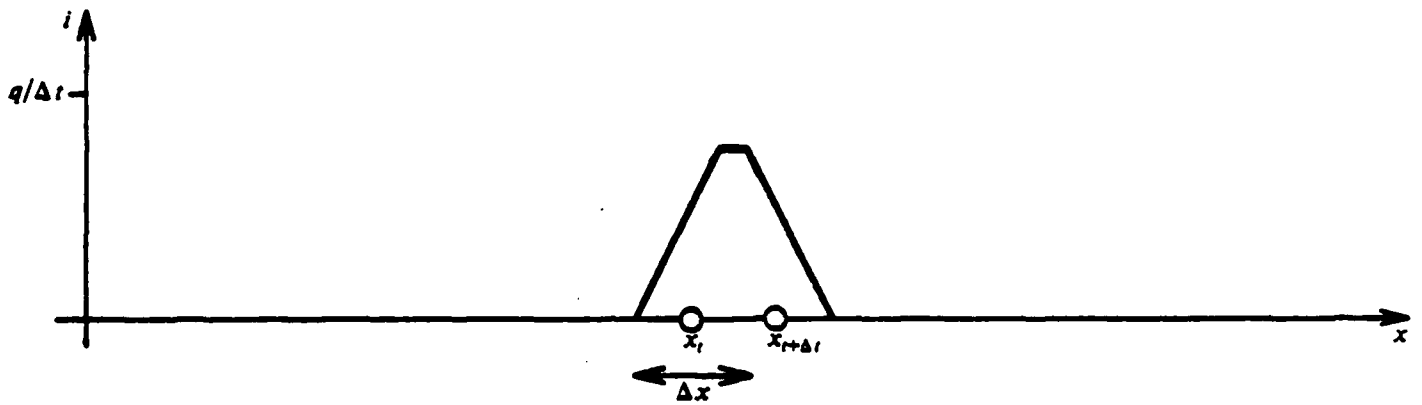


Figure 9 (Section 3.5.1.2): Current shape (slow particle).

need to know the currents everywhere at each time step. (In fact, the resulting plot would be so overfull of information that it would be almost entirely black!) So, these computations are performed only once every  $nth/5$  time steps, where  $nth$  is the number of time steps between history plots; in other words, each three-dimensional plot of the ballistic currents will have six curves  $i(x)$ .

On the other hand, we also want history plots of the boundary charge fluxes (emitter, cathode and anode fluxes). Here it would be insufficient just to compute the ballistic currents every  $(nth/5)$ th time step, but since these currents are related to particles passing isolated grid planes, the problem of constructing the current shapes is no more relevant, and the computation is now vectorizable. Consequently, the boundary charge fluxes are evaluated independently (from the ballistic currents in the whole diode) in a second part of the subroutine.

### 3.5.2. Computation of the Displacement Currents

Displacement currents are in fact computed in FIELDS, but we first needed to introduce the current shapes (Section 3.5.1.2), in order to explain why these variations of the electric field are evaluated at  $x=\Delta x$  and  $x=L-\Delta x$  instead of  $x=0$  and  $x=L$ .

Let us look at an example. We consider a single particle just about to enter the diode at  $x=0$ ; we assume that  $x_{t_0} \leq -\Delta x/2$ , and that  $-\Delta x/2 \leq x_{t_0+\Delta t} \leq 0$ . Then, the electric field due to this particle at times  $t_0$  and  $t_0+\Delta t$  is zero at both times (Figure 10), so that

$$J_{disp} = \frac{E(t_0+\Delta t) - E(t_0)}{\Delta t}$$

However, as one can see in Figure 11, the charge flux that we obtain by using the method described in Section 3.5.2.1 is nonzero at the emission plane.

So, in order to reduce this discrepancy between the ballistic and displacement currents, all "boundary" currents are computed one grid cell inside the diode (not on the boundary themselves). Consequently, we call:

- emitter charge flux:  $i=dq/dt$  due to particles passing  $X_2=\Delta x$  with  $v_x > 0$ ;
- anode charge flux:  $i=dq/dt$  due to particles passing  $X_{VG}=L-\Delta x$  with  $v_x > 0$ ;
- cathode charge flux:  $i=dq/dt$  due to particles passing  $X_2=\Delta x$  with  $v_x < 0$ ;
- currents at emitter: ballistic, displacement and total currents at  $X_2=\Delta x$ ;
- currents at target: ballistic, displacement and total currents at  $X_{VG}=L-\Delta x$ .

### 3.6. REPACK

The number of particles in the system is not constant in time. However, some arrays in the code have sizes proportional to the total number of simulated particles. Hence we must define the sizes of these arrays in such a way that we never attempt to load particles beyond the limits of the arrays. On one hand, a straightforward solution to this question is to repack the arrays from time to time, and to expand them whenever we try to go above their upper bounds. On the other hand, we could declare their sizes to be much larger than the initial number of particles, adding new particles at the end of the area (of the array) already occupied by other particles. The first solution is very costly, and the second one sets a very stringent limit on the number of time steps allowed in one run.

The REPACK subroutine executes the following compromise: the size of the arrays are chosen equal to (or greater than) the maximum number of particles that will ever be simultaneously in the system. Then, the contents of the arrays are repacked every  $ipack$ th time step, where  $ipack$  is given as an input parameter (a typical value is  $ipack=8$ ).

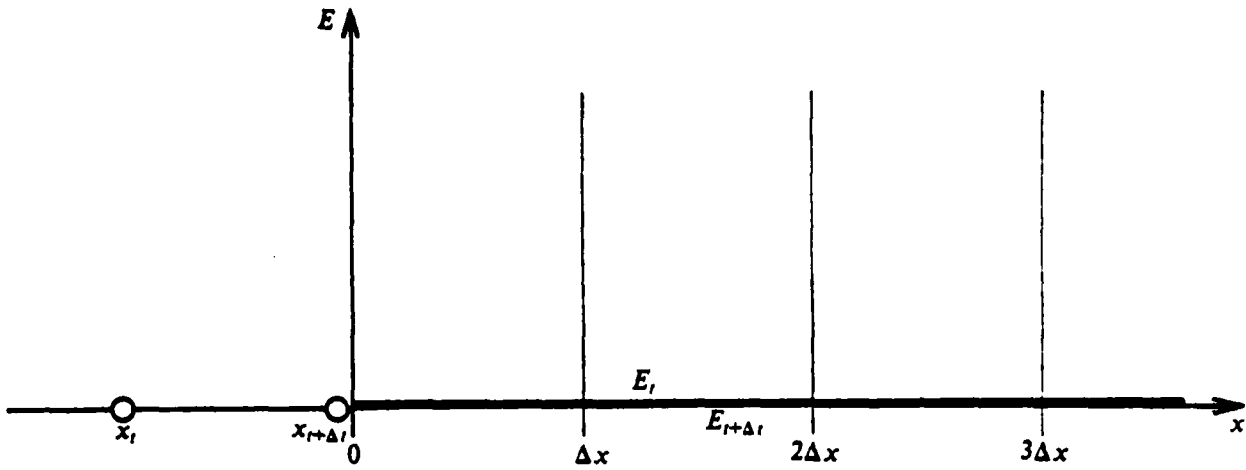


Figure 10 (Section 3.5.2): Electric fields due to a particle entering the diode.

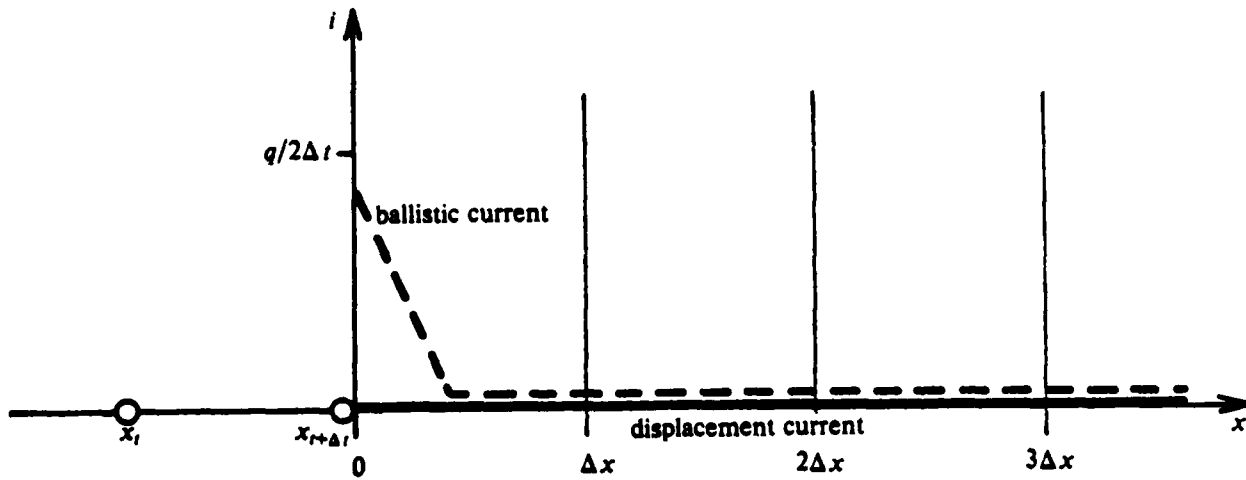


Figure 11 (Section 3.5.2): Currents due to a particle entering the diode.

### 3.7. ENTER

The role of the ENTER subroutine is to load new particles into the system during the simulation. The velocities of the entering particles are those computed in SETVNU, and their initial positions have been evaluated in SETXNU.

With this method, we see that entering particles have the same *nenter* initial velocities at each time step. This does not take into account the noise effects due to the existence of a semi-infinite plasma reservoir in the half-space  $x < 0$ , and it results in a multibeam injection, rather than a smooth one (averaged over time). This problem has been reduced by the introduction of a small noise (different at each time step) in the distribution. This noise is introduced in the form of a randomization added to the velocities given by SETVNU; the amplitude of this noise (i.e. the amount of randomization added) is given by the input parameter *randvx* (see Section 4.1.1).

### 3.8. Input Parameters

PLOUF allows the user to control a large number of physical and simulation-related variables. We describe here briefly the most important of these parameters.

#### Definition of the system:

*dt* length of the time step;  
*l* physical length of the true sheath;  
*ng* number of grid cells;  
*nt* number of time steps during the whole simulation;  
*phi0* externally applied potential, which can be time-dependent (see Figure 12);  
*phi0(1,j)* is the *j*th given value of  $\Phi_0$ ;  
*phi0(2,j)* is the time  $t_1$  when  $\Phi_0 \equiv \text{phi0}(1,j)$  must be reached;  
*phi0(3,j)* defines the evolution of  $\Phi_0(t)$  between times  $t_0 = \text{phi0}(2,j-1)$  and  $t_1 = \text{phi0}(2,j)$ .  
*randvx* percentage of noise added to the ordered velocities.

#### Definition of each species:

*nenter* number of new particles at each time step;  
*qm* charge-over-mass ratio;  
*vinbim* drift velocity of the Maxwellian (in the reservoir);  
*vinmax* maximum velocity of entering particles;  
*vinmin* minimum velocity of entering particles;  
*vinth* thermal velocity of entering particles;  
*wp* plasma frequency  $\omega_p$ .

### 3.9. Diagnostics

PLOUF gives essentially two kinds of graphic outputs: snapshots, which give the states of the sheath at some given instants, and history plots, which describe the time-evolution of different variables.

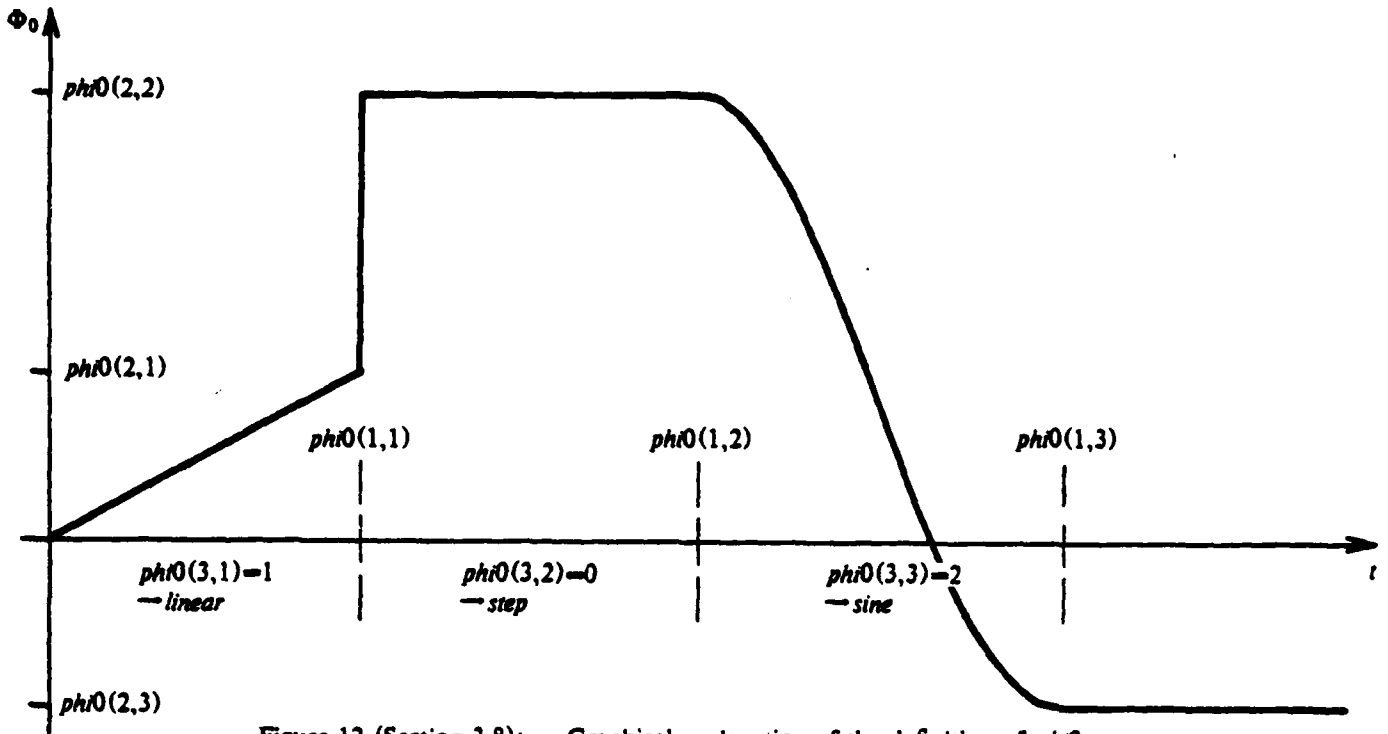


Figure 12 (Section 3.8): Graphical explanation of the definition of  $\phi i 0$ .

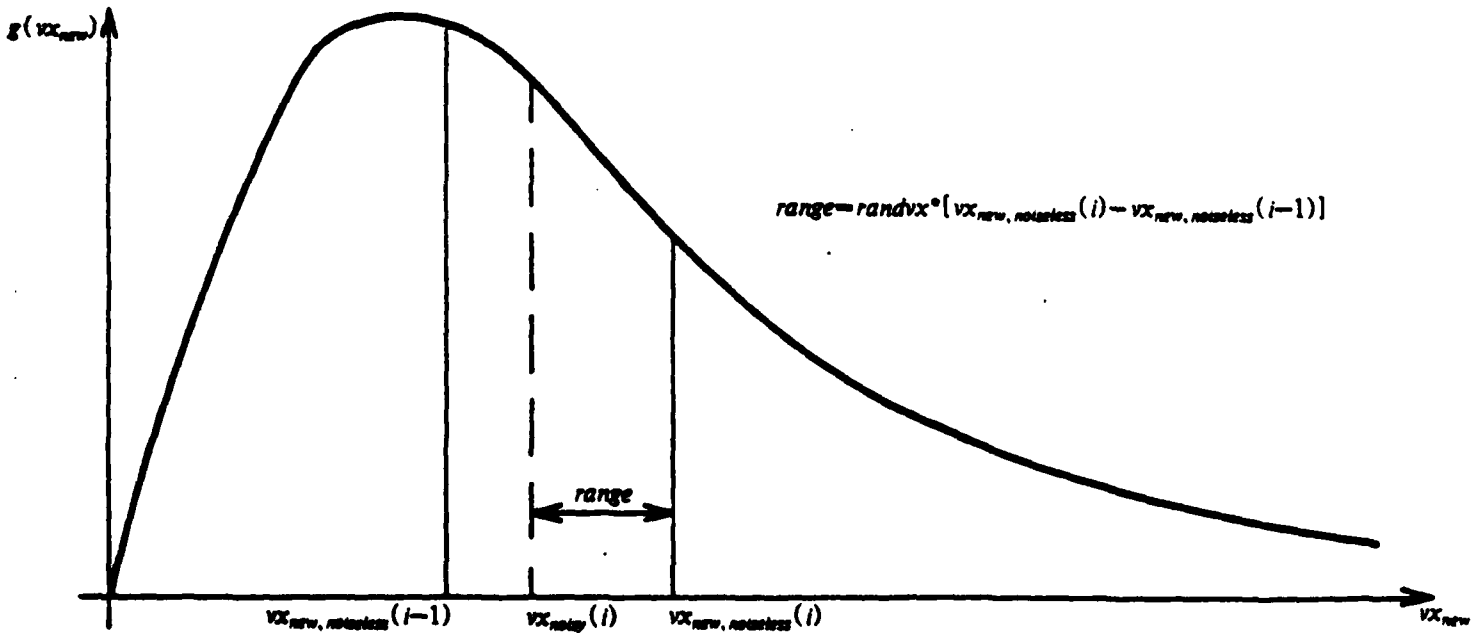


Figure 13 (Section 4.1.1): Graphical explanation of the definition of  $randvx$ .

### 3.9.1. Snapshots

The snapshots in PLOUF are the same as in ES1. They are mainly:

- charge density  $\rho$  as a function of position  $x$ ;
- electric potential  $\Phi(x)$ ;
- electric field  $E(x)$ ;
- positions of particles in phase-space  $(x, v_x)$ ;
- velocity distribution  $f(v_x)$ .

## 3.9.2. History Plots

We list below the diagnostics given by the history plots in our code (the plots marked with an "\*" are new features not to be found in ES1):

- \* externally applied potential  $\Phi_0(t)$ : this displays the time-evolution of  $\Phi_0(t)$  as prescribed by the input array *phi0*.
- \* plasma frequency  $\omega_p(t)$ : gives the plasma frequency averaged over the whole diode, as a function of time;
- \* potential minimum  $\Phi_{\min}(x,t)$ : shows the time-evolution of the position  $x$  and the value  $\Phi_{\min}$  of the minimum of the potential. (This minimum is interpolated between three neighboring grid points.)
- \* charge fluxes  $i(x_j,t)$ : shows the time-evolution of  $i(x_j)$ .
- \* emitter charge flux: plots the ballistic current due to particles passing through the grid plane at  $X_2=\Delta x$  with positive velocities.
- \* anode charge flux: plots the ballistic current due to particle passing through the grid plane at  $X_{NG}=L-\Delta x$
- \* cathode charge flux: plots the ballistic current due to particles passing through the grid plane at  $X_2=\Delta x$  with negative velocities.
- \* charge fluxes at boundaries: groups together the previous three plots, on the same scale. Note: all the charge flux plots, except  $i(X_j,t)$ , can be displayed separately for each particle species and/or for all species together.
- \* currents at emitter: plots the ballistic, displacement and total currents at  $X_2=\Delta x$ .
- \* currents at target: plots the ballistic, displacement and total currents at  $X_{NG}=L-\Delta x$ .

- field energy: 
$$E_F(t) = \sum_k \frac{\rho(k)\Phi(k)}{2}.$$

- kinetic energy: 
$$E_K(t) = \sum_i \frac{m_i v_i^2}{2}.$$

- drift energy: 
$$E_D(t) = \sum_i \frac{m_i \bar{v}_i^2}{2}.$$

- thermal energy: 
$$E_T(t) = \sum_i \frac{m_i (\overline{v_i^2} - \bar{v}_i^2)}{2}.$$

- total energy: 
$$E_Z(t) = E_F + E_K.$$

## 4. RESULTS

### 4.1. Numerical Results

#### 4.1.1. Initial Velocity Distribution and Noise

As mentioned earlier (in section 3.2.1), particles entering the sheath at  $x=0$  have their velocities chosen so as to simulate a (possibly drifting) Maxwellian distribution for  $x < 0$ , with possible randomization. The amount of added noise is controlled by the input parameter  $randvx$ , the effects of which we want to discuss now.

$randvx$  is what we define as the percentage of noise added to the regular Maxwellian. If  $v_{x_{new, noiseless}}(i-1)$  and  $v_{x_{new, noiseless}}(i)$  are two neighboring velocities of the noiseless Maxwellian defined in part 3.2.1, then  $randvx$  allows choice of  $v_{x_{noisy}}(i)$  (the initial velocity actually assigned to the particle) randomly between these values using the algorithm

$$v_{x_{new, noisy}}(i) = v_{x_{new, noiseless}}(i) - \{v_{x_{new, noiseless}}(i) - v_{x_{new, noiseless}}(i-1)\} randvx .$$

Figure 13 shows that  $randvx$  defines, for each  $v_{x_{new, noiseless}}(i)$ , the range of velocities within which  $v_{x_{noisy}}(i)$  will be randomly chosen.

Of course, such a noise will increase the noise levels of other quantities measured within the diode. However, if  $randvx$  is kept reasonably low ( $randvx=1$  is OK in many cases), the physical results are generally unchanged qualitatively. The disadvantage of adding noise is obvious (adding noise is noisy!); it may however be desirable to do so in order to suppress nonphysical diagnostics.

Figure 14 shows that too small a value of  $randvx$  yields a multistreaming phenomenon in phase-space: each line corresponds to one velocity in the noiseless Maxwellian.

Figure 15 shows that the addition of a small noise yields a much more physically plausible diagnostic: particles are indeed confined to some regions in phase-space, but  $v_x(x)$  is an infinitely-multiple-valued function of  $x$ .

Figure 16 shows how rapidly (and beautifully) the equilibrium current is reached (time  $t=0$  is in the back,  $t=5$  is in the front).

Figure 17 shows that the equilibrium is still reached very rapidly (see section 4.2.2), but that it remains very noisy when  $randvx \neq 0$ .

The above results show that it may be desirable to add noise for some purposes, whereas it just gives dirtier results in other cases. We have also found multistreaming in phase-space to be a nonphysical effect.

#### 4.1.2. Oscillations of the Potential Minimum (Driftless Case)

Previous results showed that, for a Maxwellian with no beam component (i.e. nondrifting) in the reservoir, the equilibrium solution is non-oscillatory.

However our own results almost always display some kind of time-dependence of the equilibrium state, which can be seen in the variation (in amplitude and position) of the potential minimum  $\Phi_{min}$  (Figure 18). Even though this variation is quite periodic in some instances, a closer look at it shows that it is not a physical phenomenon, but a numerical effect due to the lack of resolution inherent to our simulations.

Looking at the motion of  $\Phi_{min}$  in  $(x, \Phi)$ -space, we have noticed the following effects:

- The oscillation of  $\Phi_{min}$  occurs around the values obtained on the basis of Langmuir's findings.
- The  $x$ -variation of  $\Phi_{min}$  spans only a few inter-particle spaces, generally two or three. This

```
1D PLASMA SIMULATION 08/23/82 21:39:42
BOX B44          FIGURE 14
NIPRIO = 0.87,   IE = 0,       IFVX = 0,       IPACK = 8,
IPHI = 0,        IRHO = 0,     IRHOS = 0,     IXVY = 0,
IXYX = 500,     JANODE = .FALSE, JCATOD = .FALSE, JEMITR = .FALSE,
JTOTAL = .FALSE, NPRIO = 0,    NRANK = 5,
MPLOT = 0,
$END
A1 = 0.0,       A2 = 0.0,       DT = 0.005,     EPSI = 1.0,
IW = 2,         L = 3.141593, NG = 512,     NSP = 1,
NT = 500,       RANDVX = 0.0,     VEC = .TRUE,
PHIO = 0.0,0.0,0.0,
$END
MODE = 1,       N = 0,       MENTER = 256,   NMAX = 131072,
QM = -1.0,     THETAY = 0.0, THETAX = 0.0,   YINBIM = 0.0,
YINMAX = 1.0E+10, YINMIN = 0.0, YINTH = 5.0,     YTI = 0.0,
YT2 = 0.0,     VO = 0.0,     YI = 0.0,       WC = 0.0,
WP = 1.0,     X1 = 0.0,
$END
```

PLASMA SHEATH SIMULATION IN 1D

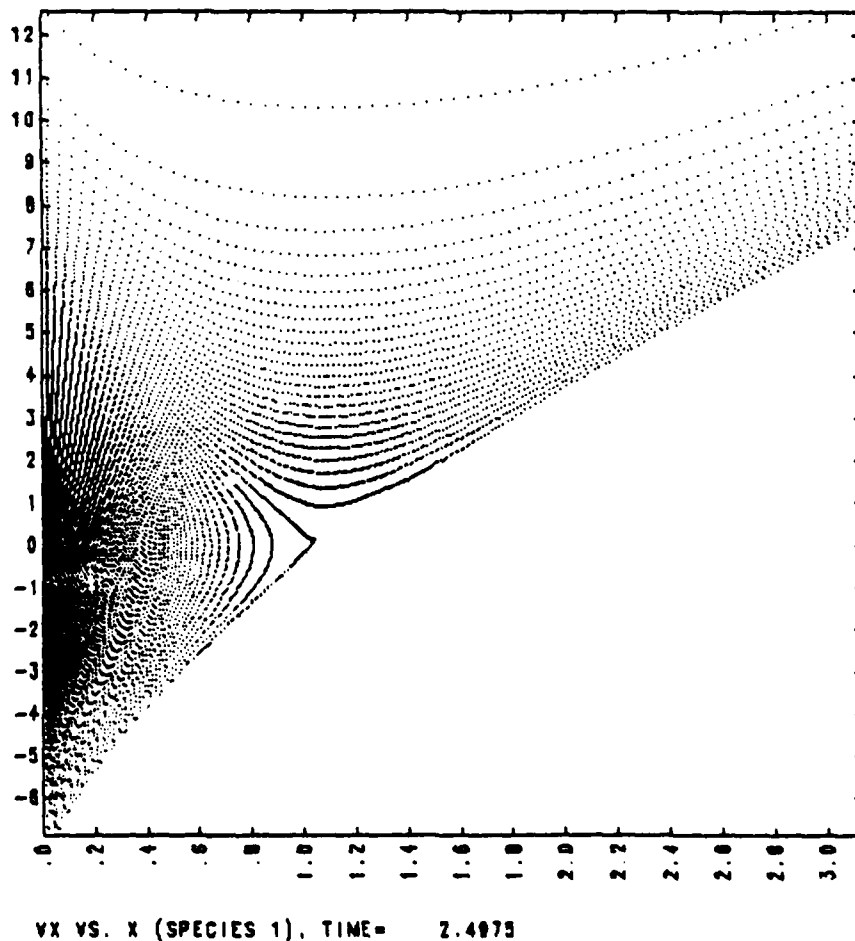


Figure 14 (Section 4.1.1): A typical distribution of particles in phase-space, for  $randvx=0$ .

```
1D PLASMA SIMULATION 08/23/82 22:29:22
BOX 844          FIGURE 15
HIPRIO = 0.87,  IE = 0,      IFVX = 0,      IPACK = 8,
IPHI = 0,      IRHO = 0,     IRHOS = 0,     IVXY = 0,
IXYX = 500,    JANODE = .FALSE, JCATOD = .FALSE, JEMITR = .FALSE,
JTOTAL = .FALSE, NPRIO = 0,  NRANK = 5,
MPLOT = 0,
$END
A1 = 0.0,      A2 = 0.0,      DT = 0.005,     EPSI = 1.0,
IW = 2,        L = 3.141593,  NG = 512,      NSP = 1,
NT = 500,      RANDVX = 1.0,     VEC = .TRUE,
PHIO = 0.0,0.0,0.0,
$END
MODE = 1,      M = 0,      MENTER = 256,  NMAX = 131072,
QM = -1.0,     THETAV = 0.0, THETAX = 0.0,  VINBIM = 0.0,
VINMAX = 1.0E+10, VINMIN = 0.0, VINTH = 5.0,   VT1 = 0.0,
VT2 = 0.0,    VO = 0.0,    V1 = 0.0,     VC = 0.0,
MP = 1.0,     X1 = 0.0,
$END
```

PLASMA SHEATH SIMULATION IN 1D

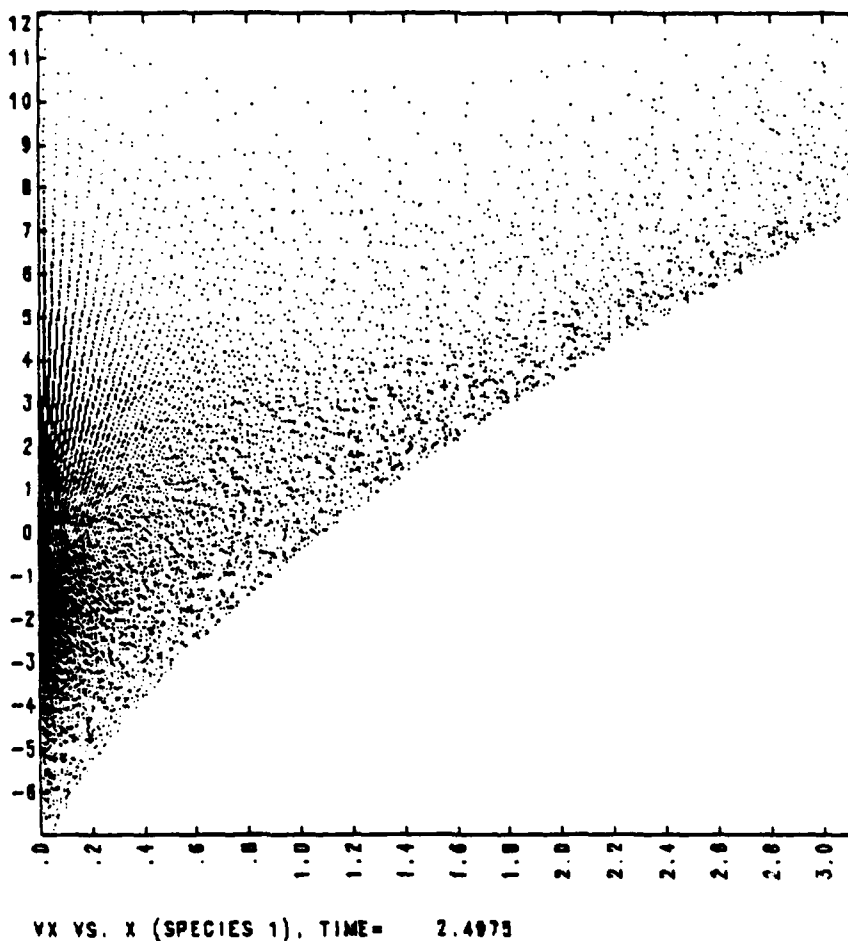
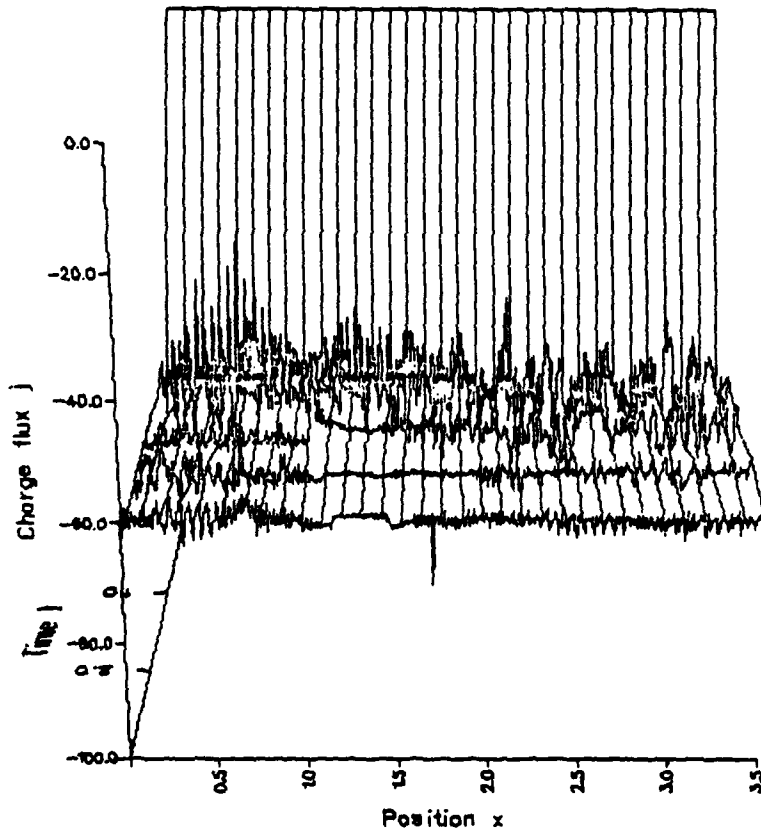


Figure 15 (Section 4.1.1): A typical distribution of particles in phase-space, for  $randvx \neq 0$ .

```
1D PLASMA SIMULATION 08/23/82 22:52:50
BOX B44          FIGURE 16
MIPRIO = 0.87,   IE = 0,       IFVX = 0,       IPACK = 8,
IPHI = 0,       IRHO = 0,     IRHOS = 0,     IXYX = 0,
IXYX = 0,       JANODE = .FALSE, JCATOD = .FALSE, JEMITR = .FALSE,
JTOTAL = .FALSE, NPRI0 = 0,   NRANK = 5,
MPL0T = 0,
$END
A1 = 0.0,       A2 = 0.0,     DT = 0.005,    EPSI = 1.0,
IW = 2,         L = 3.141593, MO = 512,    NSP = 1,
NT = 500,       RANDVX = 0.0,    VEC = .TRUE,
PH10 = 0.0,0.0,0.0,
$END
MODE = 1,       N = 0,         NENTER = 256,   NMAX = 131072,
QM = -1.0,     THETAV = 0.0,   THETAX = 0.0,  YINBIM = 0.0,
YINMAX = 1.0E+10, YINMIN = 0.0,  YINTH = 5.0,   VT1 = 0.0,
VT2 = 0.0,     VO = 0.0,     V1 = 0.0,     WC = 0.0,
WP = 1.0,     XI = 0.0,
$END
```

PLASMA SHEATH SIMULATION IN 1D



Q-FLUXES (ALL SPECIES TOGETHER), TIME= 0.0000 TO 2.5000

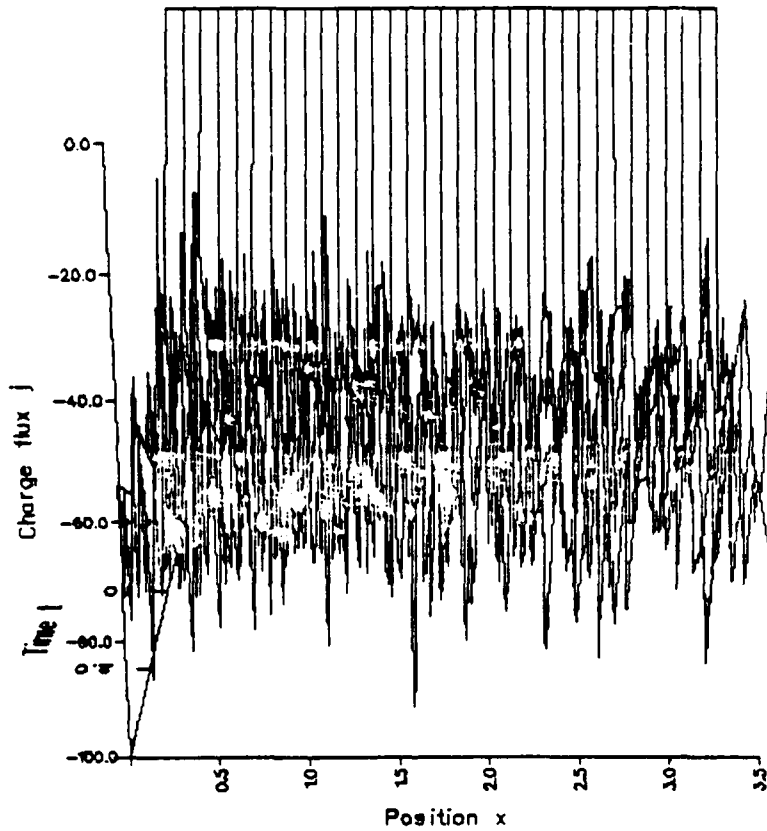
Figure 16 (Section 4.1.1): Ballistic currents before and during equilibrium, for  $randvx=0$ .

```

1D PLASMA SIMULATION 08/24/82 00:04:45
BOX 844          FIGURE 17
HIPRIO = 0.87,   IE = 0,      IFVX = 0,      IPACK = 8,
IPHI = 0,       IRHO = 0,    IRHOS = 0,    IVXY = 0,
IXYX = 0,      JANODE = .FALSE, JCATOD = .FALSE, JEMITR = .FALSE,
JTOTAL = .FALSE, NPRIO = 0,  MRANK = 5,
MPLDT = 0,
$END
A1 = 0.0,      A2 = 0.0,      DT = 0.005,    EPSI = 1.0,
IW = 2,        L = 3.141593, NG = 512,    NSP = 1,
NT = 500,      RANDVX = 1.0,  VEC = .TRUE,
PHIO = 0.0,0.0,0.0,
$END
MODE = 1,      N = 0,      NENTER = 256,  NMAX = 131072,
QM = -1.0,     THETAY = 0.0, THETAX = 0.0,  VINBIM = 0.0,
VINMAX = 1.0E+10, VINMIN = 0.0,  VINTH = 5.0,   VTI = 0.0,
VT2 = 0.0,    VO = 0.0,   V1 = 0.0,     WC = 0.0,
WP = 1.0,     X1 = 0.0,
$END

```

PLASMA SHEATH SIMULATION IN 1D



Q-FLUXES (ALL SPECIES TOGETHER), TIME= 0.0000 TO 2.5000

Figure 17 (Section 4.1.1): Ballistic currents before and during equilibrium, for  $randvx \neq 0$ .

```
1D PLASMA SIMULATION 08/24/82 14:24:53
BOX 844          FIGURE 18
HIPRIO = 0.87,  IE = 0,      IFVX = 0,      IPACK = 8,
IPHI = 0,      IRHO = 0,     IRMS = 0,     IVXY = 0,
IXVX = 0,      JANODE = .FALSE, JCATOD = .FALSE,  JEMITR = .FALSE,
JTOTAL = .FALSE, NPRI0 = 0,  NRANK = 5,
MPL0T = 0,
$END
A1 = 0.0,      A2 = 0.0,     DT = 0.005,    EPSI = 1.0,
IW = 2,        L = 3.141593,  NG = 512,     NSP = 1,
NT = 1500,     RANDVX = 0.0,    VEC = .TRUE,
PHI0 = 0.0,0.0,0.0,
$END
MODE = 1,      N = 0,      NENTER = 1024,  NMAX = 131072,
QM = -1.0,     THETAY = 0.0,  THETAX = 0.0,  VINBIM = 0.0,
VINMAX = 1.0E+10, VINMIN = 0.0,  VINTH = 5.0,   VTI = 0.0,
VT2 = 0.0,     VO = 0.0,     V1 = 0.0,     WC = 0.0,
WP = 1.0,     XI = 0.0,
$END
```

PLASMA SHEATH SIMULATION IN 1D

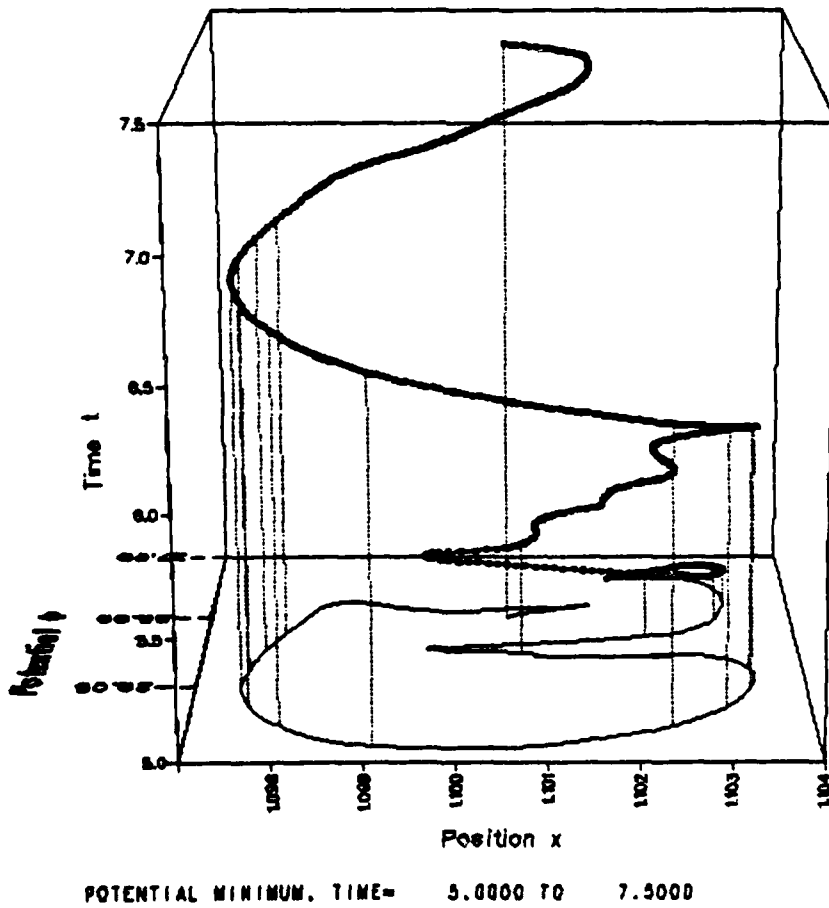


Figure 18 (Section 4.1.2): Numerical oscillation of the potential minimum.

means that, with the particle densities we had (corresponding to simulation runs with 10,000 to 100,000 particles), the position of  $\Phi_{\min}$  was basically depending on information furnished by only three or four neighboring particles. This is a very crude way of finding the true potential minimum.

\* The amplitude of the variation of  $\Phi_{\min}$  decreases when the number of particles increases, i.e. when the particle density around  $x_{\Phi_{\min}}$  increases (Figure 19). This is in part a consequence of the previous observation.

\* The behavior of  $\Phi_{\min}$  is not very sensitive to the number of grid cells.

The above results show that the variations of  $\Phi_{\min}$  and  $x_{\Phi_{\min}}$  are essentially a consequence of the coarseness of the simulation. Increasing the number of particles and decreasing  $\Delta t$ , we tend asymptotically towards a time-independent state. Thus these oscillations of the potential minimum are a numerical effect.

Note: this oscillation has never been found to give rise to (numerical) particle trapping. Indeed, a necessary condition for a particle to be trapped due to the motion of  $\Phi_{\min}$  is that the trajectory of  $\Phi_{\min}(x, t)$  has two maxima in  $x_{\Phi_{\min}}, \Phi_{\min}$ -space (Figure 20); but in our case, this trajectory has only one maximum (Figure 21), thus forbidding any trapping.

### 4.1.3. Time-Dependence of the Currents

#### 4.1.3.1. Current Noise

We have seen in Section 4.1.1 that the currents become noisier when *randvx* is increased. Our data show that the emitter, anode and cathode current noises have an essentially-linear dependence on *randvx*.

We have also compared the noises of these three boundary charge fluxes measured with the  $i=dq/dt$  method described in part 3.4.2.2, with their values measured with a zeroth-order method (i.e. one in which the ballistic currents are computed assuming point-particles). We found our own method to decrease the noises by factors of 2 to 100; the higher the particle velocities at the boundaries, the lower our improvement factor.

#### 4.1.3.2. Current Oscillations

One can easily see from Sections 3.5.1.2 and 3.5.2 that the measured currents are sensitive to the grid spacing  $\Delta x$  and the length of the time step  $\Delta t$ , as well as to the particle density and the particle velocities at the plane where we measure the currents.

So, whenever some kind of oscillatory solution is found from the simulations, chances are that it is a numerical phenomenon, not a physical one, if any one of the following conditions is met:

- if  $\Delta t$  is doubled, then the frequency of the oscillation is halved, and its amplitude is doubled;
- if  $\Delta x$  is doubled, then the frequency of the oscillation is doubled, and its amplitude is halved;
- if the particle density is doubled, then the frequency of the oscillation is doubled, and its amplitude is halved;
- if the average particle velocity around the plane used to measure the currents is doubled, then the frequency of the oscillation is doubled, and its amplitude is halved.

If all the above tests are negative, then the oscillation is most likely some kind of physical effect.

Note: the reader may have noticed that the oscillation of the potential minimum, as described in Section 4.1.2, would have failed the test for Conditions 1 and 3.

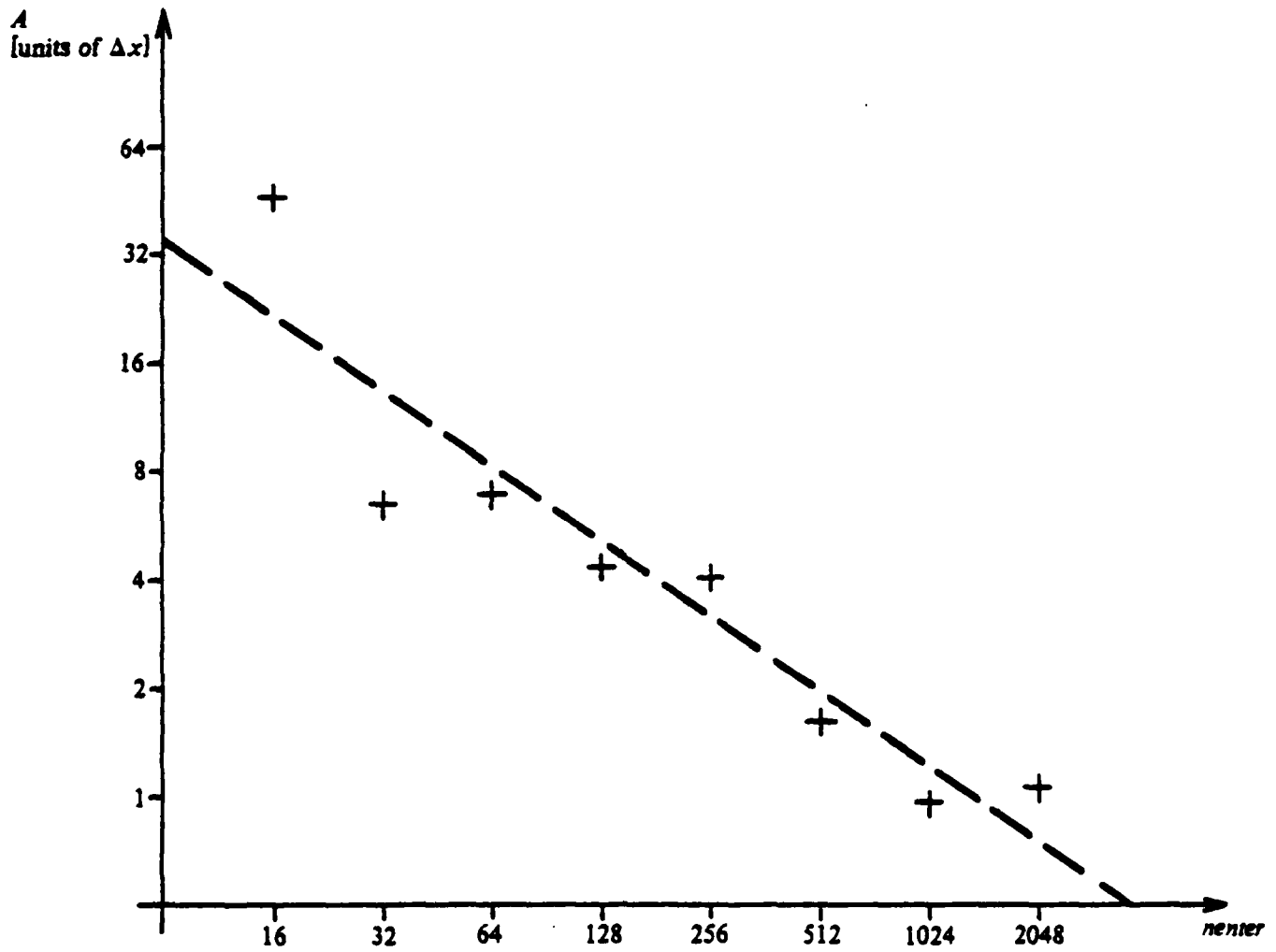


Figure 19 (Section 4.1.2): Amplitude  $A$  of the motion of the potential minimum, as a function of the particle density.

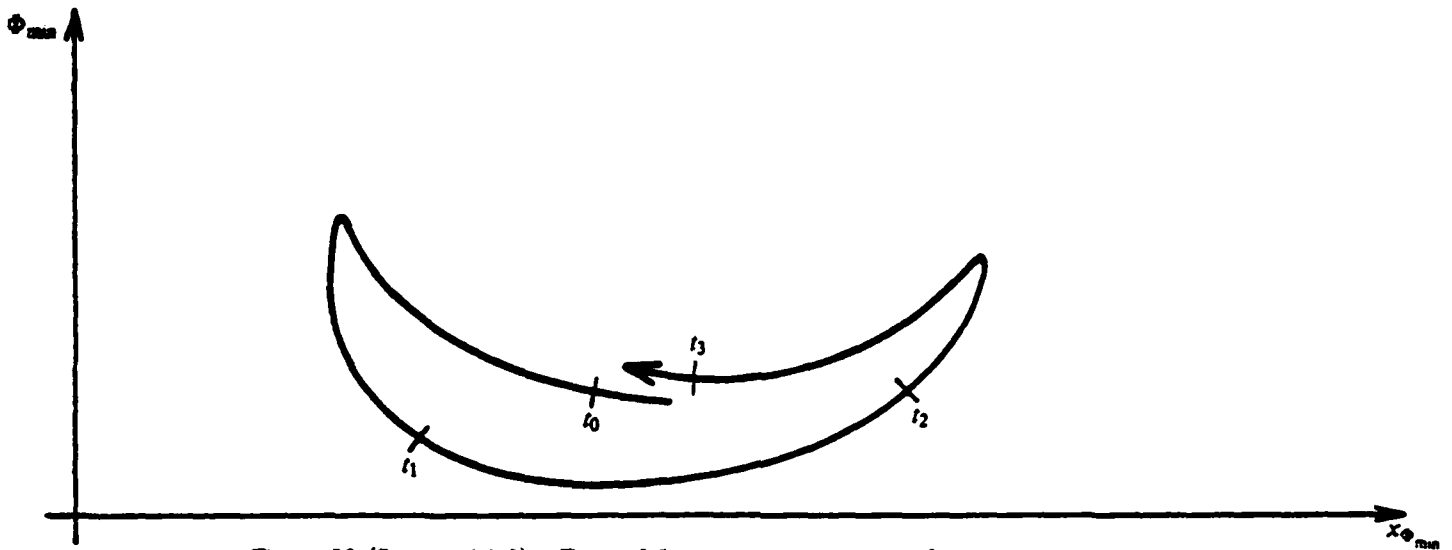


Figure 20 (Section 4.1.2): Type of  $\Phi_{\min}$ -trajectory required for particle trapping.

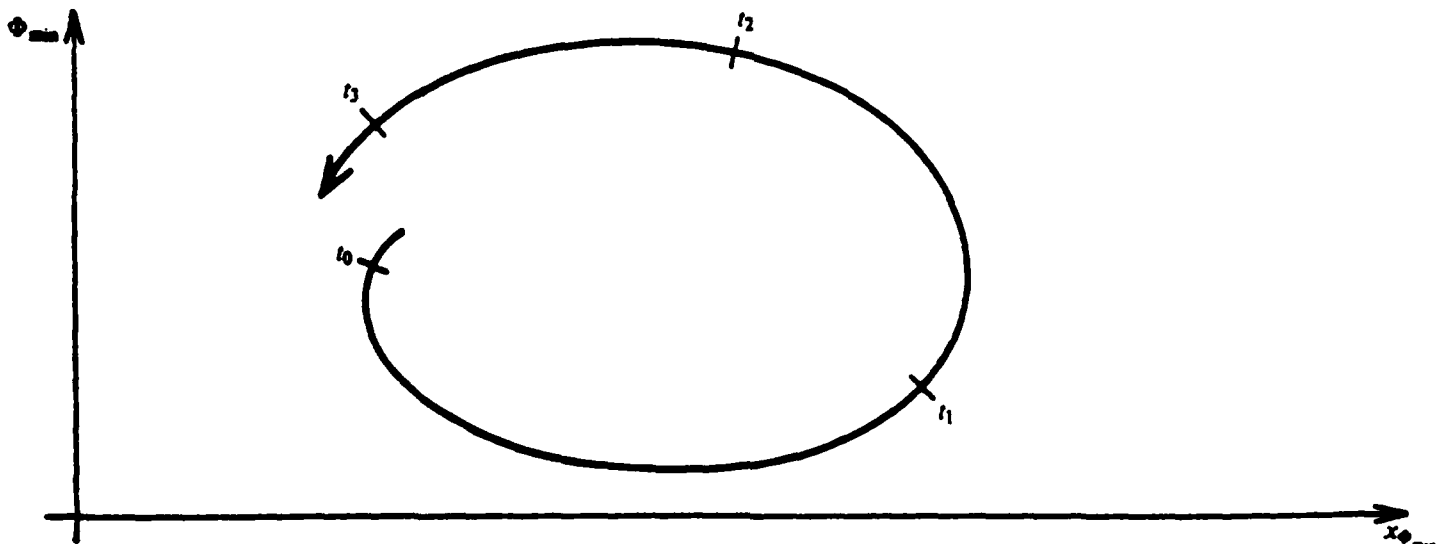


Figure 21 (Section 4.1.2): Type of  $\Phi_{\min}$ -trajectory observed in our simulations.

#### 4.1.4. Cost of the Pad-Cells

We call *pad-cells* these cells of length  $\Delta x/2$  that we add at both ends of the true sheath in order to have correct current diagnostics at the boundaries (see Section 3.5.1.2).

The cost of adding such cells is reflected into an increase of the total number of particles. Since  $\Delta x = L/ng$ , this cost increase will obviously depend on  $ng$ . We find this increase to range from 5% (for  $ng=16384$ , with  $L=\pi$ ) to 33% (for  $ng=64$ ) of the initial computation cost.

The charge flux measurement method described in section 3.5.1.2 causes a dependence of the current noise on the grid spacing: increasing the number of cells increases the noise level. We found  $ng=512$  to be the best compromise; in this case, the pad-cells represent an increase of about 7% of the computation costs.

## 4.2. Physical Results

### 4.2.1. Vacuum Diode

The well-known Child's law has been successfully verified (cold injection,  $E(0)=0$ ):

$$\Phi(x) = \Phi_0(x/L)^{4/3}.$$

Furthermore, we simulated the classical, warm, space-charge-limited diode, with half-Maxwellian injection, and compared our *particle* code diagnostics with *analytic* results obtained by William Lawson, based on steady-state diode theory as developed originally by Langmuir. Lawson used a simple program package (not a simulation code) to find the potential and other relevant quantities inside a unidimensional (plane) diode for a limited set of parameters; for his analysis, he had to follow Langmuir and assume that the potential had a *minimum* somewhere inside the diode.

We computed the positions and values of the potential minimum  $\Phi_{\min}$  for a set of different input values. Our results agreed quite accurately with Lawson's findings. The potential minimums obtained with our simulations were all less than  $L/100$  apart from the positions predicted by Lawson: note that this was obtained with  $ng=64$ , i.e. one grid cell was more than  $L/100$ .

Figure 22 shows the potential  $\Phi(x)$  in a typical space-charge-limited diode, with  $\Phi(L) = 0$ .

### 4.2.2. Reaching Equilibrium

We measured how rapidly equilibrium was reached for time-independent  $\Phi_0$ , and tested the uniqueness (with respect to  $\Phi_0$ ) of such an equilibrium.

Let us first define our plasma frequency:

$$\omega_{p,eq} \equiv \frac{1}{L} \int_0^L \omega_p(x) \Big|_{\text{equilibrium}} dx.$$

Note that the time scales on all our (single-species) plots is not in unit of  $\omega_{p,eq}^{-1}$ , but in units of  $\omega_{p,0}^{-1}$ :

$$\omega_{p,0} \equiv \frac{1}{L} \int_0^L \omega_p(x) \Big|_{t=0} dx.$$

A rule of thumb for the plots featured in this report is:  $\omega_{p,eq} \approx 8.0 \omega_{p,0}$ .

We found that, in all time-independent cases that we tested, equilibrium is quite rapidly obtained: using  $\Delta t=0.01$  ( $\Delta t$  is the length of one time step in units of  $\omega_{p,0}^{-1}$ ), equilibrium was reached as early as three plasma periods  $T_{p,eq} \equiv \omega_{p,eq}^{-1}$ . The time required to reach equilibrium increases with  $vinbim/vinth$  (see Section 4.2.3).

```
1D PLASMA SIMULATION 08/23/82 21:38:21
BOX B44          FIGURE 22
HIPRIO = 0.87,   IE = 0,       IFVX = 0,       IPACK = 8,
IPHI = 500,     IRHO = 0,     IRHOS = 0,     IVXY = 0,
IXVX = 0,      JANODE = .FALSE, JCATOD = .FALSE, JEMITR = .FALSE,
JTOTAL = .FALSE, MPRIO = 0,   MRANK = 5,
MPLOT = 0,
$END
A1 = 0.0,      A2 = 0.0,      DT = 0.01,     EPSI = 1.0,
IW = 2,        L = 3.141593, NG = 512,          NSP = 1,
NT = 500,     RANDYX = 0.0,   YEC = .TRUE,
PHIO = 0.0,0.0,0.0,
$END
MODE = 1,      N = 0,          NENTER = 1024, NMAX = 131072,
QM = -1.0,    THETAY = 0.0,   THETAX = 0.0,  VINBIM = 0.0,
VINMAX = 1.0E+10, VINMIN = 0.0,  VINTH = 1.0,  VT1 = 0.0,
YT2 = 0.0,   YD = 0.0,   V1 = 0.0,     WC = 0.0,
WP = 1.0,    X1 = 0.0,
$END
```

PLASMA SHEATH SIMULATION IN 1D

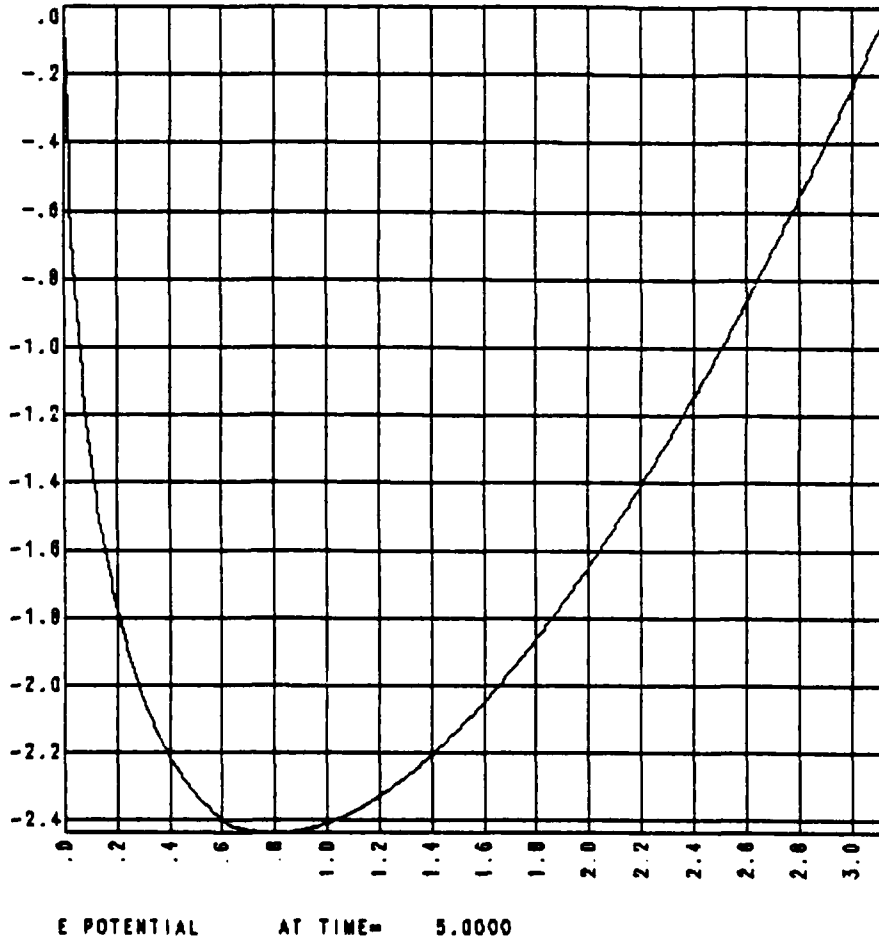


Figure 22 (Section 4.2.1): Space-charge-limited vacuum diode.

Figure 23 shows the time-variation of the total energy during the settlement of equilibrium. At  $t=2.5T_{p,0}$ ,  $\Phi_0$  is abruptly changed to show the settlement of a second equilibrium.

Figure 24 shows the motion of the potential minimum. At  $t=0$ ,  $x(\Phi_{\min})=0$  due to our initialization.  $\Phi_{\min}$  then moves towards its equilibrium position; we have shown in Section 4.1.2 that in fact  $\Phi_{\min}$  is numerically time-dependent and circles in  $(x, \Phi)$ -space around the value given by classical theory.

Figure 16 plots one curve  $i(x)$  every  $0.5T_{p,0}$ 's. The curve in the back represents the current from  $t=0$  to  $t=\Delta t$ ; the curve immediately in front of it shows the current from  $t=0.5T_{p,0}$  to  $t=0.5T_{p,0}+\Delta t$ . One sees that all curves in front of these two (i.e. obtained at later times) already correspond to an equilibrium state.

We also tested the uniqueness of equilibrium with respect to  $\Phi_0$  (i.e.: are there two or more possible equilibria for some values of  $\Phi_0$ ?). We first reached a stable equilibrium, then let  $\Phi_0$  vary slowly from its equilibrium value  $\Phi_{0,eq.}$ , then went back to  $\Phi_{0,eq.}$ ; we repeated this process for several values of  $\Phi_0$  (in particular values  $\Phi_{crit.}$  such that  $i_{anode}=0$  for  $\Phi_0=\Phi_{crit.}-\delta\Phi$  and  $i_{anode}\neq 0$  for  $\Phi_0=\Phi_{crit.}+\delta\Phi$ ). We did not find any hysteresis-like phenomenon (fortunately!); the success of this test supports our claim that the way the phase-space is filled at  $t=0$  is intrinsically irrelevant; at worst, it could lengthen the time it takes to reach equilibrium.

#### 4.2.3. Temperature Effects

Regardless of the temperature  $T$ , one has always either one of the following two cases:

- all particles reach the anode: the anode charge flux equals the emitter charge flux (at equilibrium), the potential minimum is virtually motionless, etc. The solution is completely time-independent.
- some or all of the particles contribute to the cathode charge flux: this is the case that we want to study below.

When  $i_{cathode}\neq 0$ , our simulations show that the equilibrium solution is oscillatory and undamped. Figure 25 shows the oscillation of the cathode charge flux; Figure 26 is a plot of the evolution of the potential minimum. Both results show that the particles contributing to the cathode charge flux are returned at a point which varies in time.

Figures 27 and 28 are similar diagnostics, but for  $T\neq 0$ ,  $T$  small. We see that, for  $vinth/vinbim$  small enough, we still have an oscillatory (although initially damped) solution. The damping and its duration increase with the  $vinth/vinbim$  ratio. On a series of runs with  $T=0$  and  $T$  small, it has been found that the frequency of the oscillation, whether initially damped or not, varies linearly with  $\omega_p(x_{\Phi_{\min}})$ , i.e. with the plasma frequency at the point (the position of which is time-dependent) where particles are returned to the cathode.

Now, as we further increase the temperature, damping becomes stronger, until there is virtually no more oscillation at all. Note that a damped oscillation can be obtained by giving  $vinth=0.0$ , but  $nenter\neq 1$ : even though all particles should ideally be injected at the same velocity, since  $vinth=0.0$ , they all have different real injection velocities (i.e. their velocities depend on their positions when they are counted inside the diode for the first time; but since  $nenter\neq 1$ , all entering particles at any given time step are at different positions (according to Section 3.2.2), i.e. they behave as if they had different real injection velocities. Conclusion: one should only use  $nenter=1$  when one wants to simulate a really cold case!

Finally, Figures 29 and 30 show the boundary charge fluxes and the motion of  $\Phi_{\min}$  for a warm case with no drift in the reservoir. One has then a purely time-independent solution (or, to be more accurate, what is left of time-dependence is due to noise and to the numerical effects described in Sections 4.1.2 and 4.1.3).

```
1D PLASMA SIMULATION 08/23/82 22:32:11
BOX B44          FIGURE 23
HIPRIO = 0.87,   IE = 0,       IFVX = 0,       IPACK = 8,
IPHI = 0,       IRHO = 0,     IRHOS = 0,     IVXY = 0,
IXVX = 0,       JANODE = .FALSE, JCATOD = .FALSE, JEMITR = .FALSE,
JTOTAL = .FALSE, NPRIO = 0,   MRANK = 5,
MPLOT = 0,
$END
A1 = 0.0,       A2 = 0.0,       DT = 0.01,     EPSI = 1.0,
IW = 2,         L = 3.141593, NG = 512,       NSP = 1,
NT = 500,       RANDYX = 0.0,     VEC = .TRUE,
PHIO = -4.0, 2.5, 0, 11.0, 5.0, 0,
$END
MODE = 1,       N = 0,       NENTER = 512,   NMAX = 131072,
QM = -1.0,     THETAV = 0.0, THETAX = 0.0,   VINBIM = 0.0,
VINMAX = 1.0E+10, VINMIN = 0.0, YINTH = 1.0,    YTI = 0.0,
YT2 = 0.0,    Y0 = 0.0,    Y1 = 0.0,      WC = 0.0,
WP = 0.1,     X1 = 0.0,
$END
```

PLASMA SHEATH SIMULATION IN 1D

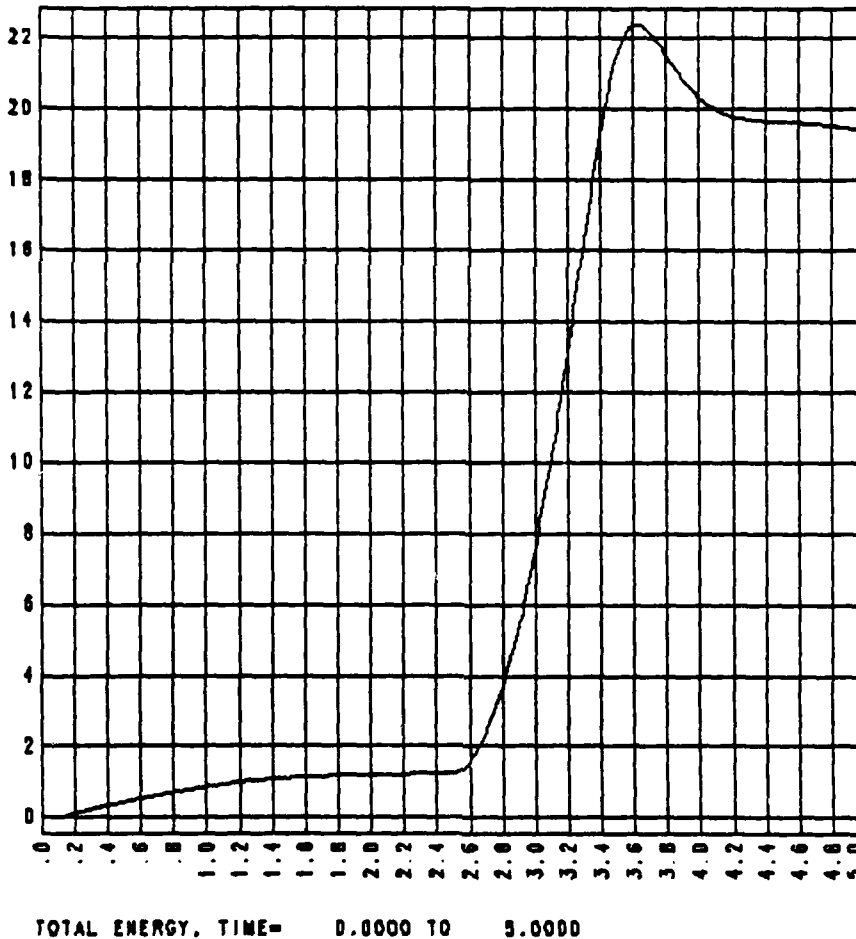


Figure 23 (Section 4.2.2): Total energy during settlement of two successive equilibria.

1D PLASMA SIMULATION 08/24/82 00:05:09

BOX B44

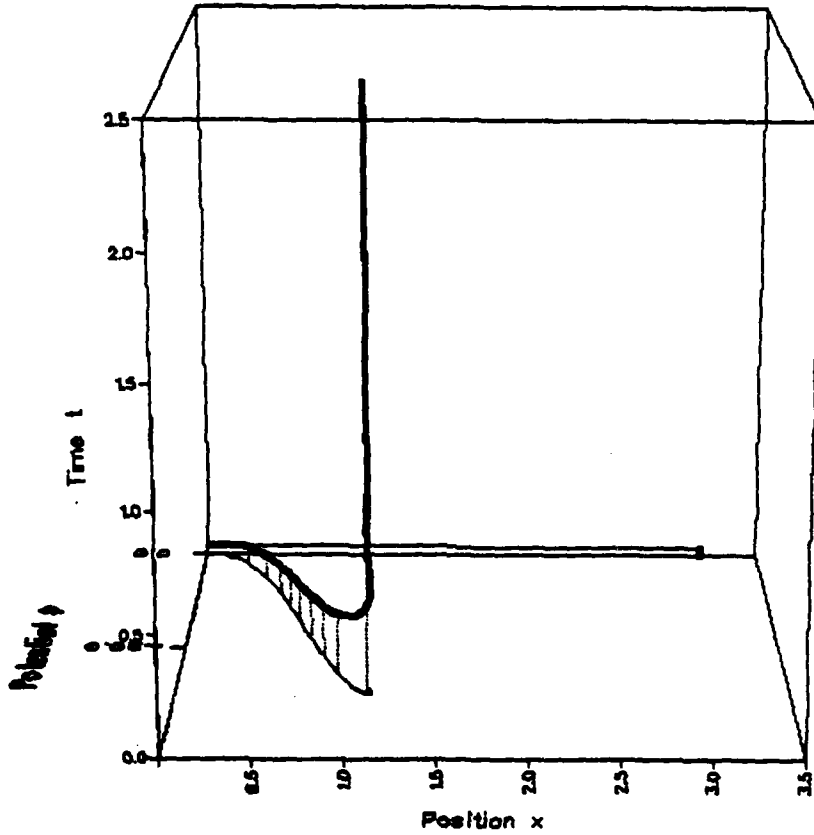
FIGURE 24

```

HIPRIO = 0.87, IE = 0, IFYX = 0, IPACK = 8,
IPHI = 0, IRHO = 0, IRHOS = 0, IVXVY = 0,
IXVX = 0, JANODE = .FALSE, JCATOD = .FALSE, JEMITR = .FALSE,
JTOTAL = .FALSE, NPRIO = 0, MRANK = 5,
NPLDT = 0,
$END
A1 = 0.0, A2 = 0.0, DT = 0.005, EPSI = 1.0,
IW = 2, L = 3.141593, NG = 512, NSP = 1,
NT = 500, RANDYX = 0.0, VEC = .TRUE,
PHIO = 0.0, 0.0, 0.0,
$END
MODE = 1, N = 0, MENTER = 1024, NMAX = 131072,
QM = -1.0, THETAY = 0.0, THETAX = 0.0, VINMIN = 0.0,
VINMAX = 1.0E+10, VINMIN = 0.0, VINTH = 5.0, VT1 = 0.0,
VT2 = 0.0, VO = 0.0, V1 = 0.0, WC = 0.0,
WP = 1.0, X1 = 0.0,
$END

```

PLASMA SHEATH SIMULATION IN 1D



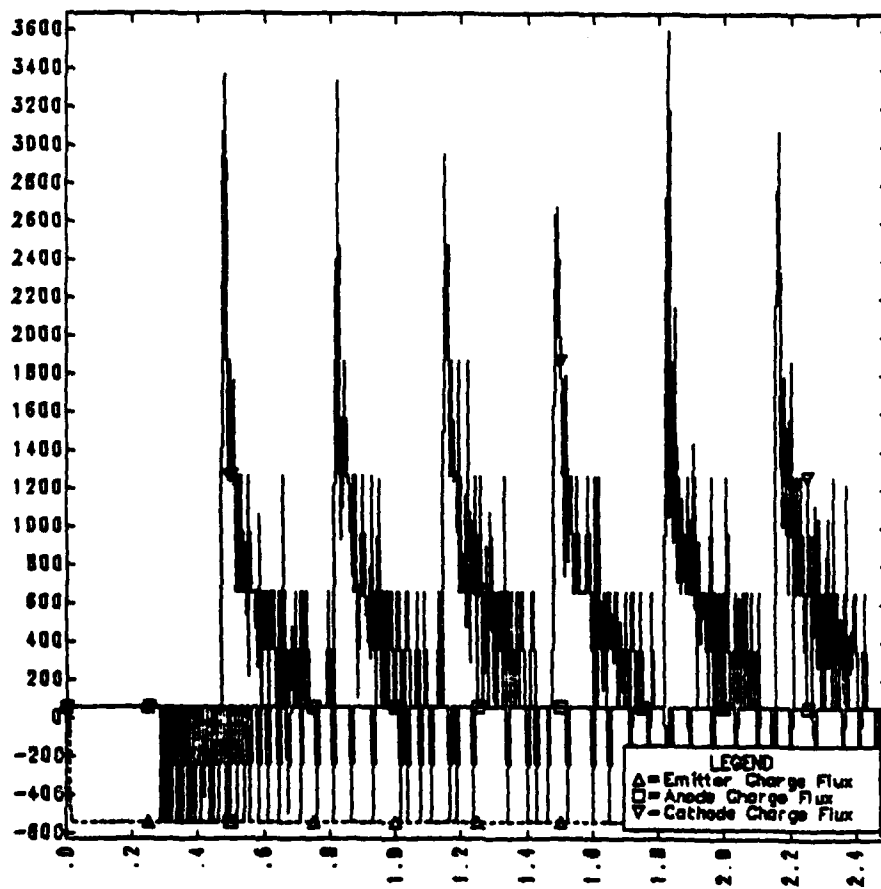
POTENTIAL MINIMUM, TIME= 0.0000 TO 2.5000

Figure 24 (Section 4.2.2):  $\Phi_{min}$  and  $x_{\Phi_{min}}$  during settlement of equilibrium.

```

1D PLASMA SIMULATION 08/24/82 00:43:59
BOX B44          FIGURE 25
HIPRIO = 0.87,  IE = 0,      IFVX = 0,      IPACK = 8,
IPHI = 0,      IRHO = 0,     IRHOS = 0,     IVXY = 0,
IXVX = 0,      JANODE = .FALSE, JCATOD = .FALSE, JEMITR = .FALSE,
JTOTAL = .FALSE, NPRIO = 0,   NRANK = 5,
NPLOT = 0,
$END
A1 = 0.0,      A2 = 0.0,      DT = 0.005,     EPSI = 1.0,
IW = 2,        L = 3.141593,  NG = 512,      NSP = 1,
NT = 1000,     RANDVX = 0.0,   VEC = .TRUE,
PHID = 0.0,0.0,0.0,
$END
MODE = 1,      N = 0,      NENTER = 1,    NMAX = 131072,
QM = -1.0,     THETAY = 0.0,  THETAX = 0.0,  VINBIM = 10.0,
VINMAX = 1.0E+10, VINMIN = 0.0,  VINTH = 0.0,   VT1 = 0.0,
VT2 = 0.0,    VO = 0.0,   V1 = 0.0,      WC = 0.0,
WP = 1.0,     X1 = 0.0,
$END
    
```

PLASMA SHEATH SIMULATION IN 1D



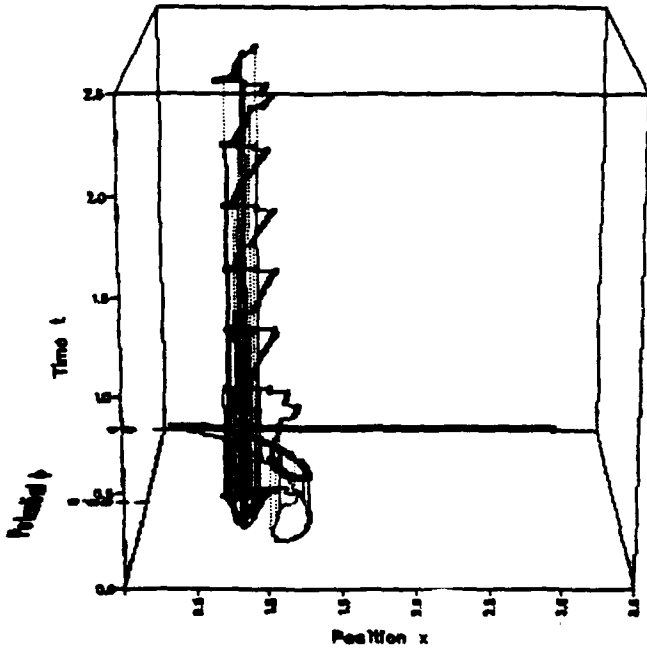
Q-FLUXES AT BOUNDARIES (SPECIES 1), TIME= 0.0000 TO 2.5000

Figure 25 (Section 4.2.3): Boundary charge fluxes in a cold, space-charge-limited diode,  $\Phi_0 = 0$ .

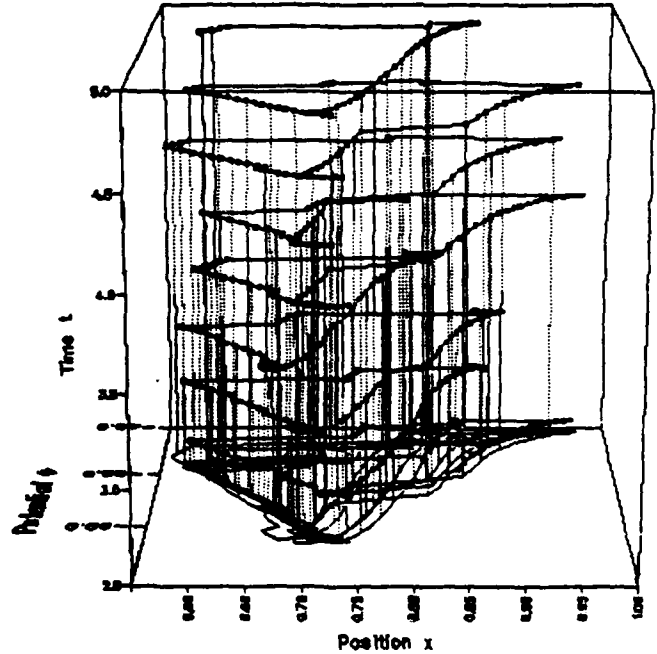
```

1D PLASMA SIMULATION 08/24/82 01:08:13
BOX B44          FIGURE 26
HIPRIO = 0.87,  IE = 0,      IFVX = 0,      IPACK = 8,
IPHI = 0,      IRHO = 0,    IRMOS = 0,   IVXY = 0,
IXVX = 0,      JANODE = .FALSE, JCATOD = .FALSE, JEMITR = .FALSE,
JTOTAL = .FALSE, NPRI0 = 0,  NRANK = 5,
MPL0T = 0,
$END
A1 = 0.0,      A2 = 0.0,    DT = 0.005,   EPSI = 1.0,
IW = 2,        L = 3.141593, NG = 512,      NSP = 1,
NT = 1000,     RANDVX = 0.0,    VEC = .TRUE,
PHI0 = 0.0,0.0,0,
$END
MODE = 1,      N = 0,      NENTER = 1,   NMAX = 131072,
QM = -1.0,     THETAV = 0.0,   THETAX = 0.0, VINBIM = 10.0,
VINMAX = 1.0E+10, VINMIN = 0.0,  VINTH = 0.0,  VT1 = 0.0,
YT2 = 0.0,    Y0 = 0.0,      Y1 = 0.0,    WC = 0.0,
WP = 1.0,     X1 = 0.0,
$END
    
```

PLASMA SHEATH SIMULATION IN 1D



POTENTIAL MINIMUM, TIME= 0.0000 TO 2.3000

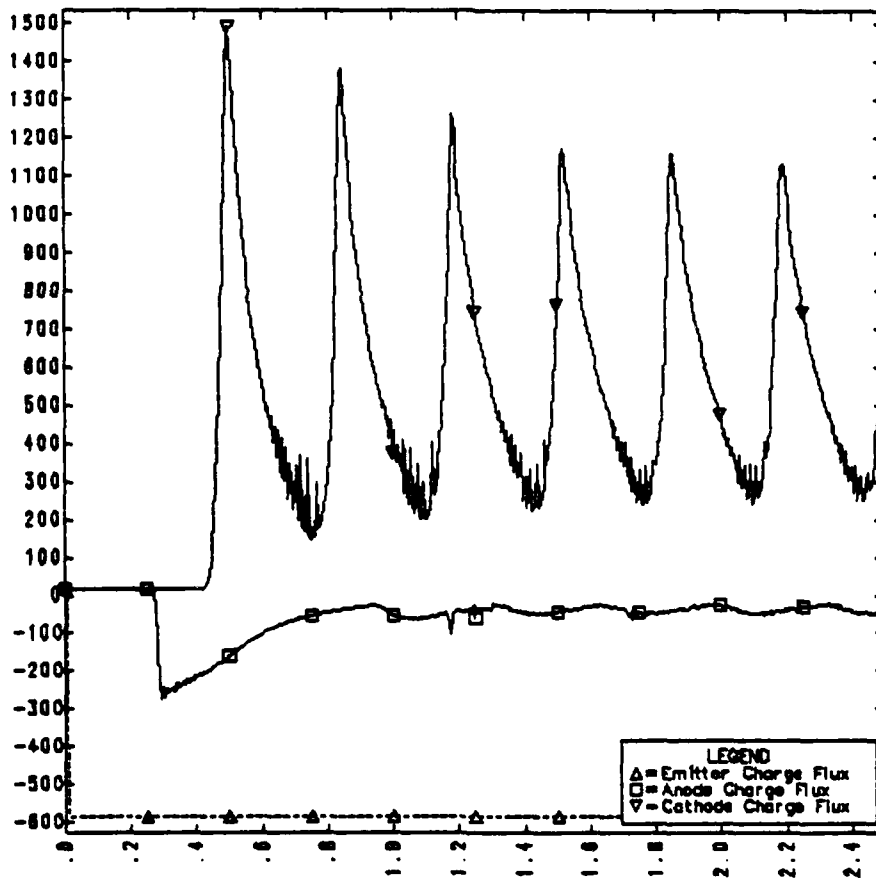


POTENTIAL MINIMUM, TIME= 2.3000 TO 5.0000

Figure 26 (Section 4.2.3): Evolution of  $\Phi_{min}$  in a cold, space-charge-limited diode.

```
1D PLASMA SIMULATION 08/24/82 01:38:15
BOX B44          FIGURE 27
HIPRIO = 0.87,   IE = 0,       IFVX = 0,       IPACK = 8,
IPHI = 0,        IRHO = 0,     IRMS = 0,      IVXVY = 0,
IXVX = 0,        JANODE = .FALSE, JCATOD = .FALSE, JEMITR = .FALSE,
JTOTAL = .FALSE, MPRIO = 0,    NRANK = 5,
MPLOT = 0,
$END
A1 = 0.0,        A2 = 0.0,      DT = 0.005,    EPSI = 1.0,
IW = 2,          L = 3.141593, NG = 512,          NSP = 1,
NT = 1000,       RANDYX = 0.0,    VEC = .TRUE,
PHIO = 0.0,0.0,0.0,
$END
MODE = 1,        N = 0,          NENTER = 1024, NMAX = 131072,
QM = -1.0,       THETAY = 0.0,    THETAX = 0.0,  VINBIM = 10.0,
VINMAX = 1.0E+10, VINMIN = 0.0,  VINTH = 0.5,   VT1 = 0.0,
YT2 = 0.0,       VO = 0.0,     V1 = 0.0,      WC = 0.0,
WP = 1.0,        X1 = 0.0,
$END
```

PLASMA SHEATH SIMULATION IN 1D



Q-FLUXES AT BOUNDARIES (SPECIES 1), TIME= 0.0000 TO 2.5000

Figure 27 (Section 4.2.3): Boundary charge fluxes in a space-charge-limited diode with  $T=0, T \neq 0$ .

10 PLASMA SIMULATION 08/23/82 21:38:58

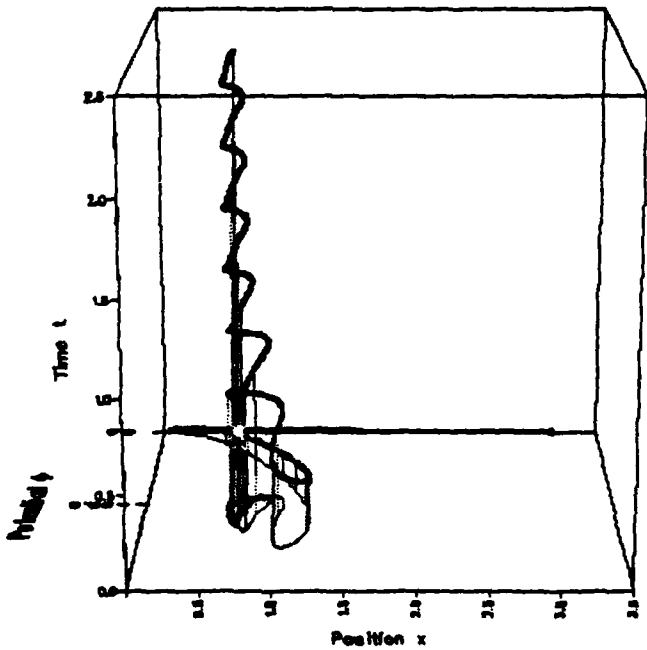
BOX B44 FIGURE 28

```

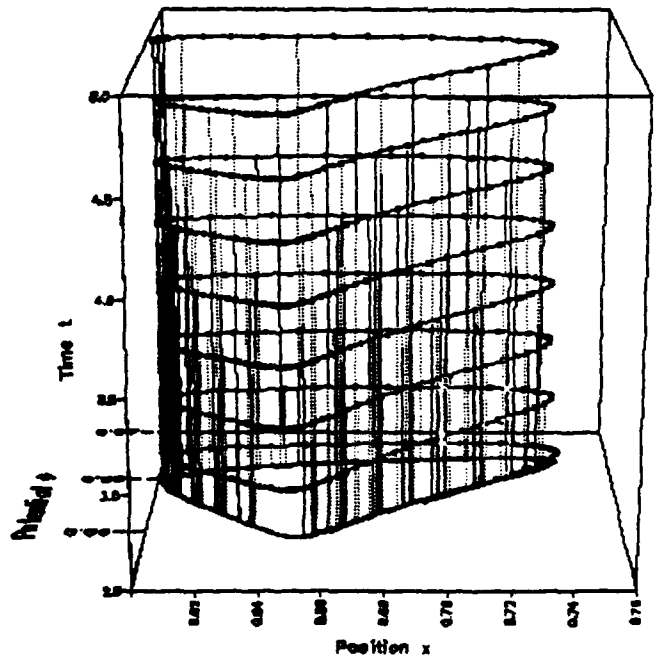
HIPRIO = 0.87, IE = 0, IFYX = 0, IPACK = 8,
IPHI = 0, IRHO = 0, IRMOS = 0, IVXY = 0,
IXYX = 0, JANOGE = .FALSE, JCATOD = .FALSE, JEMITH = .FALSE,
JTOTAL = .FALSE, NPRI0 = 0, NRANK = 5,
MPL0T = 0,
$END
A1 = 0.0, A2 = 0.0, DT = 0.005, EPSI = 1.0,
IW = 2, L = 3.141593, NG = 512, NSP = 1,
NT = 1000, RANDYX = 0.0, VEC = .TRUE,
PHI0 = 0.0,0.0,0,
$END
MODE = 1, N = 0, NENTER = 1024, NMAX = 131072,
QM = -1.0, THETAV = 0.0, THETAX = 0.0, VINBIM = 10.0,
VINMAX = 1.0E+10, VINMIN = 0.0, VINTH = 0.5, VT1 = 0.0,
VT2 = 0.0, VO = 0.0, V1 = 0.0, WC = 0.0,
WP = 1.0, X1 = 0.0,
$END

```

PLASMA SHEATH SIMULATION IN 10



POTENTIAL MINIMUM, TIME= 0.0000 TO 2.5000



POTENTIAL MINIMUM, TIME= 2.5000 TO 5.0000

Figure 28 (Section 4.2.3): Evolution of  $\Phi_{min}$  in a space-charge-limited diode with  $T=0, T \neq 0$ .

```
1D PLASMA SIMULATION 08/24/82 00:28:10
BOX B44          FIGURE 29
HIPRIO = 0.87,  IE = 0,      IFVX = 0,      IPACK = 8,
IPHI = 0,      IRHO = 0,     IRMOS = 0,     IVXY = 0,
IXVX = 0,      JANODE = .FALSE, JCATOD = .FALSE, JEMITR = .FALSE,
JTOTAL = .FALSE, NPRIO = 0,  NRANK = 5,
MPLT = 0,
$END
A1 = 0.0,      A2 = 0.0,     DT = 0.005,    EPSI = 1.0,
IW = 2,        L = 3.141593, NG = 512,         NSP = 1,
NT = 1000,     RANDVX = 0.0,        YEC = .TRUE,
PHID = 0.0,0.0,0.0,
$END
MODE = 1,      N = 0,        NENTER = 1024,  NMAX = 131072,
QM = -1.0,     THETAY = 0.0,          THETAX = 0.0,  VINBIM = 0.0,
VINMAX = 1.0E+10, VINMIN = 0.0,          VINTH = 5.0,   YI1 = 0.0,
YT2 = 0.0,    Y0 = 0.0,         V1 = 0.0,      WC = 0.0,
WP = 1.0,     X1 = 0.0,
$END
```

PLASMA SHEATH SIMULATION IN 1D

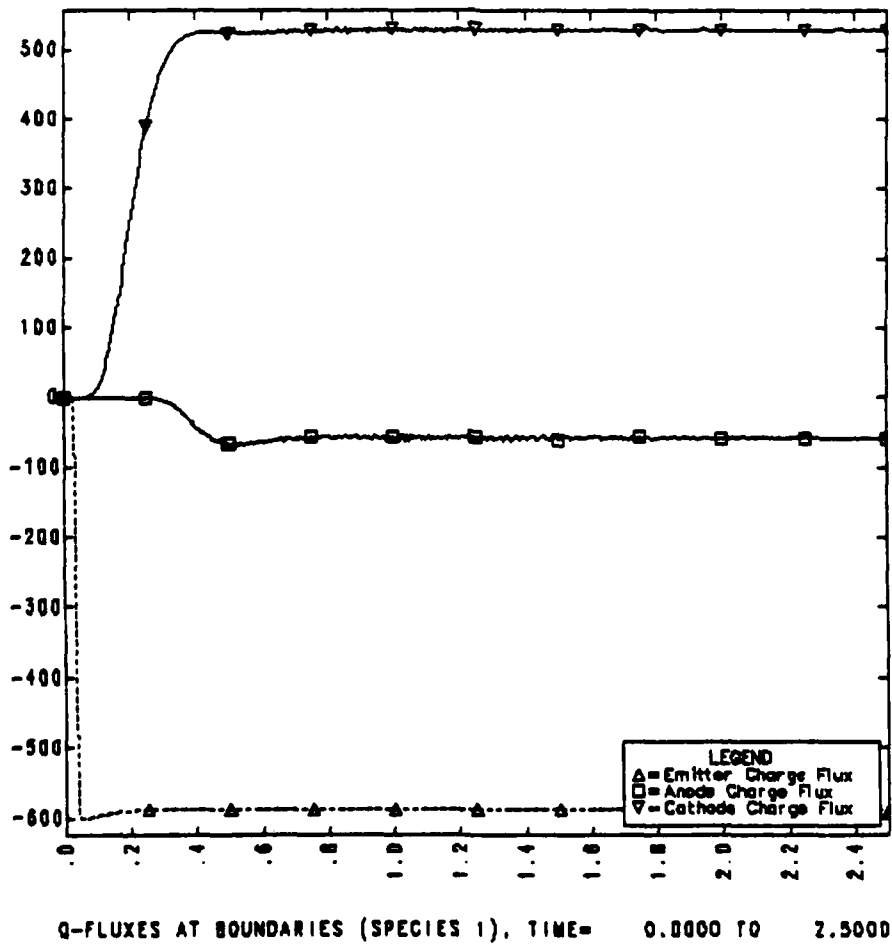
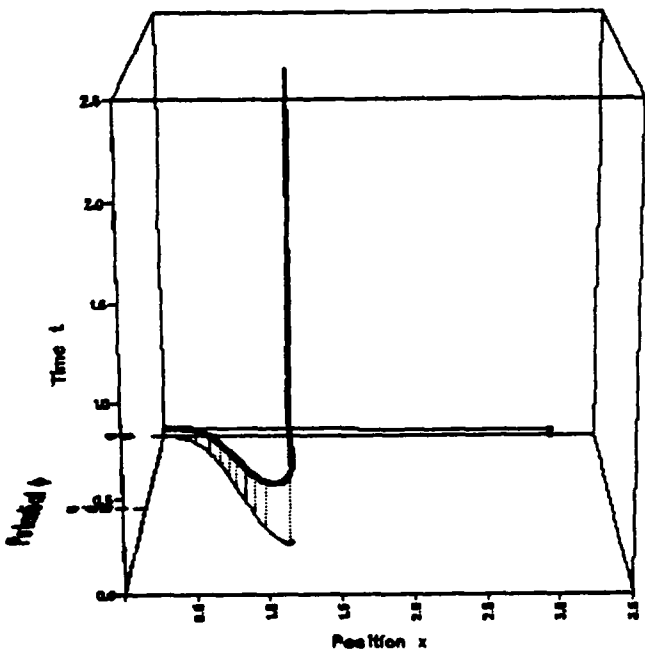


Figure 29 (Section 4.2.3): Boundary charge fluxes in a warm, space-charge-limited diode.

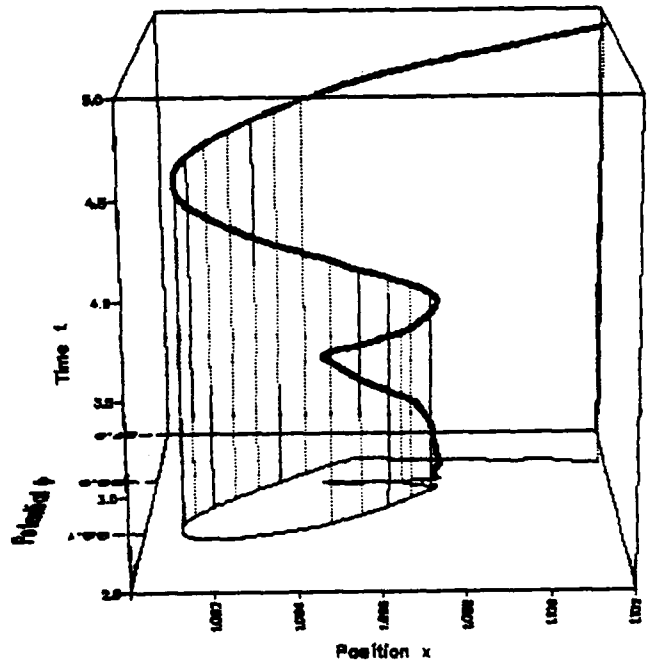
```

10 PLASMA SIMULATION 08/24/82 01:37:28
BOX 844          FIGURE 30
HIPRIO = 0.87,   IE = 0,       IFVX = 0,       IPACK = 8,
IPHI = 0,        IRHO = 0,     IRHOS = 0,     IXYY = 0,
IXVX = 0,        JANODE = .FALSE, JCATOD = .FALSE, JEMITR = .FALSE,
JTOTAL = .FALSE, NPRIO = 0,    NRANK = 5,
MPLOT = 0,
$END
A1 = 0.0,        A2 = 0.0,     DT = 0.005,    EPSI = 1.0,
IW = 2,          L = 3.141593, NG = 512,        NSP = 1,
NT = 1000,      RANDYX = 0.0,    VEC = .TRUE,
PHID = 0.0,0 0.0,
$END
MODE = 1,        N = 0,       NENTER = 1024,  NMAX = 131072,
QM = -1.0,      THETAY = 0.0, THETAX = 0.0,  YINBIM = 0.0,
VINMAX = 1.0E+10, VINMIN = 0.0, VINTH = 5.0,   VT1 = 0.0,
YT2 = 0.0,      YO = 0.0,    V1 = 0.0,      WC = 0.0,
NP = 1.0,       X1 = 0.0,
$END
    
```

PLASMA SHEATH SIMULATION IN 1D



POTENTIAL MINIMUM, TIME= 0.0000 TO 2.5000



POTENTIAL MINIMUM, TIME= 2.5000 TO 5.0000

Figure 30 (Section 4.2.3): Evolution of  $\Phi_{\min}$  in a warm, space-charge-limited diode.

#### 4.2.4. Effect of $\Phi_0$ on the Velocity Distribution

When  $\Phi_0$  increases, less and less particles will be reflected back to the cathode, and the average velocity will increase. More high-energy particles will be present in the system at each instant.

Figure 31 shows the Maxwellian distribution of velocities for a totally-reflecting  $\Phi_0$  ( $i_{anode}=0$ ).

In figure 32,  $\Phi_0$  is much larger than in the previous case; this can be deduced from the presence of a hot tail in the distribution of velocities.

This confirms the obvious fact that particles receive energy during their transit time in the diode, provided the balance current is nonzero ( $i_{anode} \neq 0$ ).

#### 4.2.5. $i=i(\Phi_0)$ Characteristic

The S-shaped curve giving  $i$  as a function of  $\Phi_0$  is well-known: for  $\Phi_0$  small enough,  $i_{anode}=0$ ; then, as  $\Phi_0$  increases,  $i_{anode}$  becomes nonzero, and increases with  $\Phi_0$ , until it reaches a saturation value above which  $i_{anode}=i_{emitter}$ .

Figure 33 shows  $i_{anode}(\Phi_0)$  and  $i_{cathode}(\Phi_0)$ . The high noise levels and the almost straight shapes of the currents are due to the fact that, for graphics purpose, we let  $\Phi_0(t)$  increase fairly rapidly in time, whereas the theoretical S-curve is obtained for  $\Phi_0 \neq \Phi_0(t)$ . Also,  $\omega_p$  is time-varying, since the average density within the sheath varies; this means that on this plot  $\Phi_0$  does not increase linearly with  $t$ .

Other simulation runs made on larger time-scales have given much "cleaner" results, agreeing quite well with theory.

```
1D PLASMA SIMULATION 08/24/82 04:08:48
BOX B44          FIGURE 31
HIPRIO = 0.87,  IE = 0,      IFYX = 500,   IPACK = 8,
IPHI = 0,      IRHO = 0,    IRHOS = 0,   IVXY = 0,
IXVX = 0,      JANODE = .FALSE, JCATOD = .FALSE, JEMITR = .FALSE,
JTOTAL = .FALSE, NPRI0 = 0,  HRANK = 5,
MPL0T = 0,
$END
A1 = 0.0,      A2 = 0.0,    DT = 0.01,   EPSI = 1.0,
IW = 2,        L = 3.141593, NG = 512,     NSP = 1,
NT = 500,      RANDVX = 0.0, VEC = .TRUE,
PHID = -4.0,0.0,0.0,
$END
MODE = 1,      N = 0,      NENTER = 512,  NMAX = 131072,
QM = -1.0,     THETAV = 0.0, THETAX = 0.0,  VINBIM = 0.0,
VINMAX = 1.0E+10, VINMIN = 0.0, VINTH = 1.0,   YT1 = 0.0,
VT2 = 0.0,    VO = 0.0,   V1 = 0.0,     WC = 0.0,
WP = 0.1,     X1 = 0.0,
$END
```

PLASMA SHEATH SIMULATION IN 1D

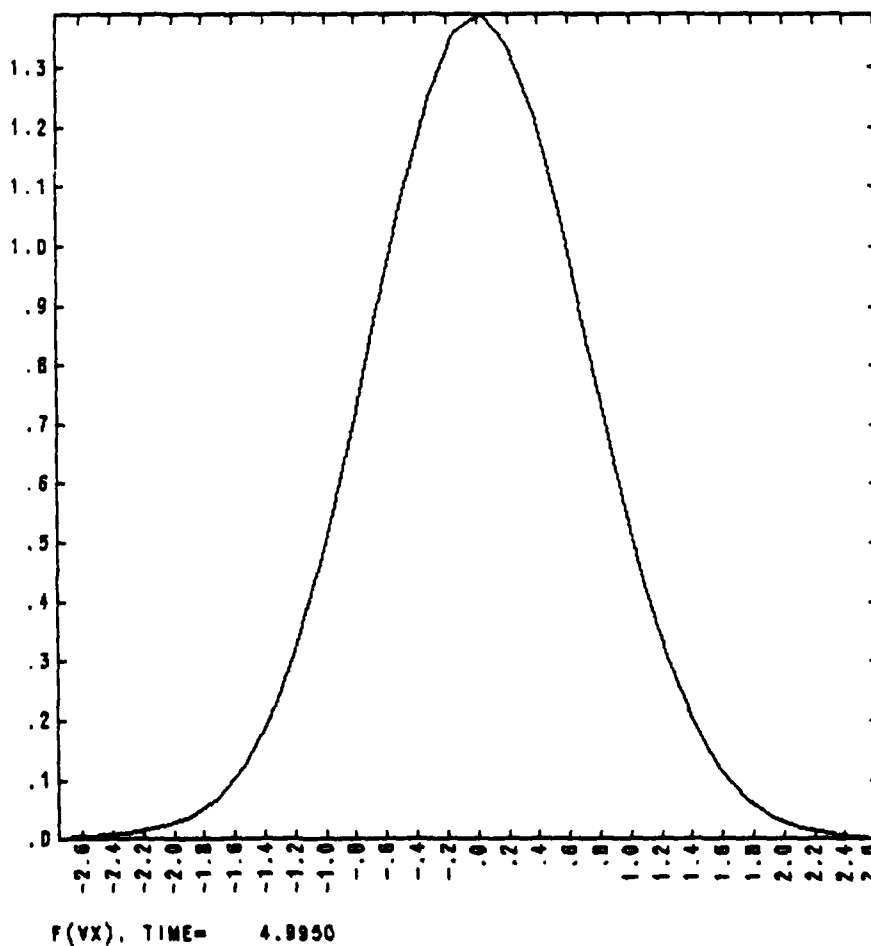


Figure 31 (Section 4.2.4):  $f(v_x)$  in the diode for  $\Phi_0$  reflecting all particles.

```
10 PLASMA SIMULATION 08/24/82 09:02:51
BOX B44          FIGURE 32
HIPRIO = 0.87,  IE   = 0,      IFVX  = 500,   IPACK = 8,
IPHI   = 0,     IRHO  = 0,     IRHOS = 0,   IVXY  = 0,
IXVX   = 0,     JANODE = .FALSE, JCATOD = .FALSE, JEMITR = .FALSE,
JTOTAL = .FALSE, NPRIO = 0,    NCRANK = 5,
MPLLOT = 0,
$END
A1     = 0.0,   A2     = 0.0,   DT    = 0.01,  EPSI  = 1.0,
IW     = 2,    L      = 3.141593, NG    = 512,   NSP   = 1,
NT     = 500,  RANDYX = 0.0,   VEC   = .TRUE,
PHIO   = 4.0,0.0,0.0,
$END
MODE   = 1,    N       = 0,    NENTER = 512,  NMAX  = 131072,
QM     = -1.0, THETAY = 0.0,  THETAX = 0.0,  VINBIM = 0.0,
VINMAX = 1.0E+10, VINMIN = 0.0,  VINTH  = 1.0,  VT1   = 0.0,
YT2    = 0.0,  VO     = 0.0,   V1     = 0.0,  WC    = 0.0,
WP     = 0.1,  X1     = 0.0,
$END
```

PLASMA SHEATH SIMULATION IN 10

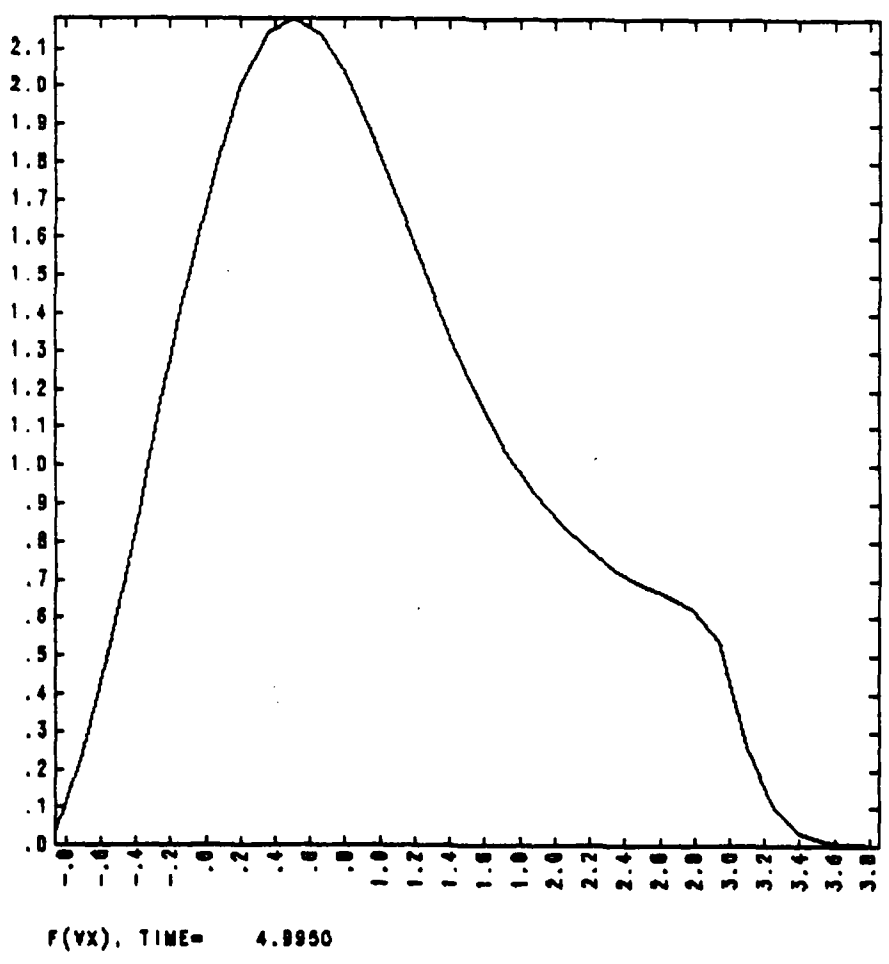
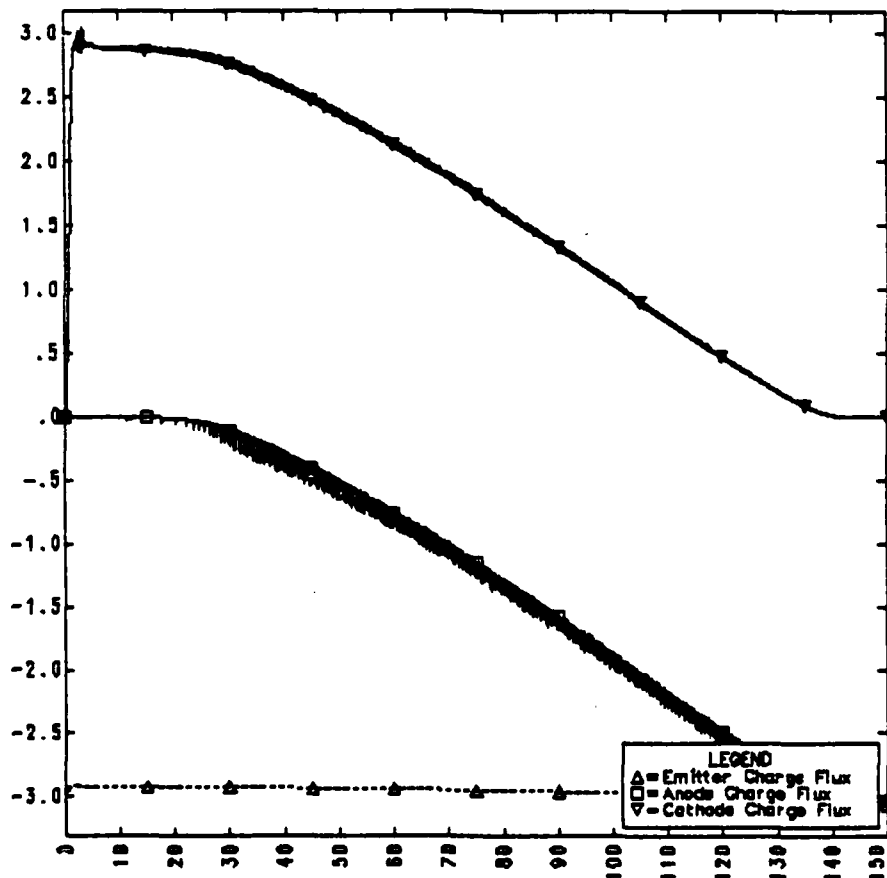


Figure 32 (Section 4.2.4):  $f(v_x)$  in the diode for  $\Phi_0$  reflecting part of the particles.

1D PLASMA SIMULATION 08/23/82 21:26:49  
BOX B44 FIGURE 33  
HIPRIO = 0.87, IE = 0, IFVX = 0, IPACK = 8,  
IPHI = 0, IRHO = 0, IRHOS = 0, IVXY = 0,  
IXVX = 0, JANODE = .FALSE, JCATOD = .FALSE, JEMITR = .FALSE,  
JTOTAL = .FALSE, NPRI0 = 0, NHRANK = 5,  
MPL0T = 0,  
\$END  
A1 = 0.0, A2 = 0.0, DT = 0.01, EPSI = 1.0,  
IW = 2, L = 3.141593, NG = 512, NSP = 1,  
NT = 15000, RANDYX = 0.0, VEC = .TRUE,  
PHIC = -4.0,5.0,0, 11.0,150.0,1,  
\$END  
MODE = 1, N = 0, NENTER = 512, NMAX = 131072,  
QM = -1.0, THETAY = 0.0, THETAX = 0.0, VINBIM = 0.0,  
VINMAX = 1.0E+10, VINMIN = 0.0, VINTH = 1.0, VT1 = 0.0,  
YT2 = 0.0, YO = 0.0, V1 = 0.0, YC = 0.0,  
WP = 0.1, X1 = 0.0,  
\$END

PLASMA SHEATH SIMULATION IN 1D



Q-FLUXES AT BOUNDARIES (SPECIES 1), TIME= 0.0000 TO 150.0000

Figure 33 (Section 4.2.5):  $i = i(\Phi_0)$ .

## 5. CONCLUSION

We believe that the goal of this project has been reached, since we have now a tool which allows us to better understand a wide range of physical phenomena in several problems related to the plasma sheath.

In the future, we expect other people and ourselves to use our code for the study of more elaborated problems involving several species, a magnetic field, possible secondary emission at the target, etc.

We hope that the basic information contained in this report will be beneficial in helping those who wish to understand our code and/or to use it.

REFERENCES

- [1] I. Langmuir, "The Effect of Space Charge and Initial Velocities on the Potential Distribution and Thermoionic Current Between Parallel Electrodes", *Phys. Rev.* 21, 419 (1923).
- [2] I. Langmuir & H. Mott-Smith, "Studies of Electric Discharges in Gases at Low Pressures", *G.E. Rev.* 27, 449 (1924).
- [3] J. R. Pierce, "Possible Fluctuations in Electron Streams Due to Ions", *J. Appl. Phys.* 19, 231 (1948).
- [4] P. K. Tien & J. Moshman, "Monte Carlo Calculation of Noise Near the Potential Minimum of a High-Frequency Diode", *J. Appl. Phys.* 27, 1067 (1956).
- [5] S. A. Self, "Exact Solution of the Collisionless Plasma-Sheath Equation", *Phys. Fluids* 6, 1762 (1963).
- [6] C. K. Birdsall & W. B. Bridges, "Electron Dynamics of Diode Regions", *Academic Press*, (1966).
- [7] A. B. Langdon & C. K. Birdsall, "Theory of Plasma Simulation Using Finite-Size Particles", *Phys. Fluids* 13, 2115 (1970).
- [8] R. K. Franklin, "Plasma Phenomena in Gas Discharges", *Clarendon Press* (1976).
- [9] S. Kuhn, "Determination of Axial Steady-State Potential Distributions in Collisionless Single-Ended Q-Machines", *Plasma Phys.* 21, 613 (1978).
- [10] C. K. Birdsall & A. B. Langdon, "Plasma Physics via Computer Simulation", *McGraw-Hill* (to be published 1983).

**MED**  
**8**